# D5.2

# EO Tools and Products – Specifications – Final

| | |
|---|---|
| Instrument | Collaborative Project |
| Call / Topic | H2020-SEC-2016-2017/H2020-SEC-2016-2017-1 |
| Project Title | Multi-Hazard Cooperative Management Tool for Data Exchange, Response Planning and Scenario Building |
| Project Number | 740689 |
| Project Acronym | HEIMDALL |
| Project Start Date | 01/05/2017 |
| Project Duration | 42 months |
| Contributing WP | WP 5 |
| Dissemination Level | PU |
| Contractual Delivery Date | M38 |
| Actual Delivery Date | 04/08/2020 |
| Editor | Sandro Martinis (DLR) |
| Contributors | Stéphanie Battiston (UNISTRA), Stephen Clandillon (UNISTRA), Claire Huber (UNISTRA), Michaela Rättich (DLR), Guido Luzi (CTTC), Maria Cuevas (CTTC), Michael Nolde (DLR), Julien Briant (UNISTRA), Mathilde Caspard (UNISTRA), Rémi Braun (UNISTRA) |

| Document History | | | |
|---|---|---|---|
| Version | Date | Modifications | Source |
| 0.1 | 13/03/20 | First draft | DLR |
| 0.2 | 22/04/20 | Second draft | DLR |
| 0.3 | 29/07/20 | QA reviewed | AVA |
| 1.0.F | 04/08/2020 | First Issue | DLR |

# Table of Contents

List of Figures ..... iv
List of Tables ..... vi
List of Acronyms ..... vii
Executive Summary ..... 10
1 Introduction ..... 11
2 Earth Observation Technical Requirements ..... 12
2.1 Interface Requirements ..... 12
2.1.1 Hardware Interfaces ..... 12
2.1.2 Software Interfaces ..... 12
2.1.3 Communication Interfaces ..... 12
2.2 Functional Technical Requirements ..... 13
2.2.1 Short-Term Features ..... 13
2.2.2 Mid-Term Features ..... 13
2.2.3 Long-Term Features ..... 14
2.3 Other Requirements ..... 15
2.3.1 Short-Term Requirements ..... 15
2.3.2 Mid-Term Requirements ..... 15
2.3.3 Long-Term Requirements ..... 15
3 Reference Architecture ..... 16
4 Module Functionality ..... 17
5 Technical Specification of the Earth Observation Processing Chains ..... 19
5.1 TerraSAR-X and Sentinel-1 Flood Service ..... 20
5.1.1 SAR-based flood detection ..... 20
5.1.2 TerraSAR-X and Sentinel-1 ..... 20
5.1.3 TerraSAR-X and Sentinel-1 flood processing chain ..... 21
5.1.4 Products ..... 24
5.2 VHR optical and Sentinel-2 flood processing chains ..... 25
5.2.1 Optical data-based flood detection ..... 25
5.2.2 VHR optical sensors and Sentinel-2 ..... 31
5.2.3 VHR optical and Sentinel-2-based flood processing chains ..... 32
5.2.4 Products ..... 35
5.3 Fire hot spot detection ..... 36
5.3.1 MODIS-based fire hot spot processing chain ..... 36
5.3.2 Products ..... 37
5.4 Burn scar mapping using Sentinel-2 ..... 37

5.4.1 Optical data-based burn scar detection ....37
5.4.2 Methodology for Sentinel-2-based burned area detection ....38
5.4.3 Products ....38
5.5 Fire Severity ....38
5.5.1 Optical data-based fire severity ....38
5.5.2 Fire severity: Methodology with SWIR channels ....39
5.5.3 Fire severity: Methodology without SWIR channels ....41
5.5.4 Fire Severity Products ....43
5.6 SAR-based landslide monitoring ....44
5.6.1 Detection of landslides using SAR data ....44
5.6.2 Sentinel-1-based landslide monitoring chain ....44
5.6.3 Products ....45
5.7 Landslide mapping using Sentinel-2 ....46
5.7.1 Detection of landslides using optical data ....46
5.7.2 Sentinel-2 landslide detection chain ....46
5.7.3 Products ....48
6 Test Plan ....52
7 Conclusions ....54
8 References ....55

# List of Figures

Figure 3-1: HEIMDALL architecture....16

Figure 4-1: Generic workflow of the processing chains of the module Earth Observation Products....17

Figure 4-2: Screenshot of the template for requesting EO-based products via the HEIMDALL GUI....18

Figure 5-1: Workflow of DLR's TerraSAR-X Flood Service (TFS) [2, modified]....23

Figure 5-2: Workflow of DLR's Sentinel-1 Flood Service (S-1FS) [1, modified]....24

Figure 5-3: Initial status of the optical data-based flood detection workflow previous to the HEIMDALL work....27

Figure 5-4: Optical data-based flood detection workflow....32

Figure 5-5: WATEX interface....33

Figure 5-6: WaToV interface....33

Figure 5-7: Current operational Sentinel-2 data-based flood detection workflow....34

Figure 5-8: Sentinel-2 water extraction - Thác Bà Lake, Vietnam, August 2019....36

Figure 5-9: Pléiades-HR water extraction - Forbes, Australia, September 2016....36

Figure 5-10: Optimal pre and post Sentinel-2 band combinations, resulting pre and post NBR's and resulting dNBR - Rognac fire event, France, August 2016....40

Figure 5-11: Deriving a dNBR based fire severity index....41

Figure 5-12: Results of different fire severity methodologies....42

Figure 5-13: Results of fire severity dNDVI methodology. The two middle classes are regrouped afterwards....43

Figure 5-14: Fire severity product based on Pléiades-HR data - La Jonquera fire event, 24/07/2012....44

Figure 5-15: Workflow of the developed methodology to produce DAM and ADA....45

Figure 5-16: SlidEx automatic landslide detection workflow for Landsat-8/Sentinel-2 data....47

Figure 5-17: SlidEx interface....47

Figure 5-18: S2 reference image (Sichuan, 19/02/2017)....49

Figure 5-19: S2 crisis image (Sichuan, 07/09/2017)....49

Figure 5-20: Landslide detection by double threshold on pre/post disaster NDVI difference and slope....49

Figure 5-21: S2 reference image (Freetown, 01/02/2017)....49

Figure 5-22: S2 crisis image (Freetown, 08/11/2017)....49

Figure 5-23: Landslide detection by double threshold on pre/post disaster NDVI difference and slope....49

Figure 5-24: S2 reference image (Kumamoto 03/03/2016)....50

Figure 5-25: S2 crisis image (Kumamoto 10/08/2016)....50

Figure 5-26: Landslide detection by double threshold on pre/post disaster NDVI difference and slope....50

Figure 5-27: S2 reference image (16/06/2018). .....50

Figure 5-28: Pléiades 1A crisis data (09/07/2018) .....50

Figure 5-29: Landslide extraction over Kure during early July 2018 rainfall (Pléiades 1-A, © CNES, distribution Airbus Defence and Space) .....51

# List of Tables

Table 2-1: Technical Requirement TR_DataEO_1.....13
Table 2-2: Technical Requirement TR_DataEO_2.....13
Table 2-3: Technical Requirement TR_DataEO_4.....14
Table 2-4: Technical Requirement TR_DataEO_3.....14
Table 5-1: Overview about the main characteristics of the EO-based processing chains.....19
Table 5-2:TerraSAR-X acquisition modes [15].....21
Table 5-3: List of global databases containing water classifications analysed within [5].....27
Table 5-4: Qualitative criteria used to classify the water databases.....28
Table 5-5: Value classes and weightings are allocated to each criterion to analyse the databases.....29
Table 5-6: Classes for criteria 1.....29
Table 5-7: Classes for criteria 2.....29
Table 5-8: Classes for criteria 3.....29
Table 5-9: Classes for criteria 4.....29
Table 5-10: Classes for criteria 5.....29
Table 5-11: Classes for criteria 6.....30
Table 5-12: Ranking of global, water surface containing, databases with respect to their pertinence in selecting samples for flood-time water body mapping .....30
Table 5-13*:* US Forest Service dNBR fire severity classification .....40
Table 5-14*:* Comparison between dNBR classes and simplified severity classes .....41
Table 5-15: Fire severity class description and corresponding dNDVI values which work for Sentinel-2 and SPOT-6/7 dNDVI calculation. .....43
Table 6-1*:* TS_EO_01.....52
Table 6-2*:* TS_EO_02.....52
Table 6-3*:* TS_EO_03.....52

# List of Acronyms

| | |
|---|---|
| ADA | Active Deformation Areas |
| ANN | Artificial Neural Networks |
| CTTC | Centre Tecnològic de Telecomunicacions de Catalunya |
| DAM | Deformation Activity Map |
| DEM | Digital Elevation Model |
| DFD | German Remote Sensing Data Center |
| DLR | Deutsches Zentrum für Luft- und Raumfahrt e.V. (German Aerospace Center) |
| EO | Earth Observation |
| EOS | Earth Observing System |
| ESA | European Space Agency |
| CNES | Centre National d'études Spatiales |
| FRP | Fire Radiative Power |
| GAM | Geohazard Activity Map |
| GRD | Ground Range Detected |
| GPT | Graph Processing Tool |
| GUI | Graphical User Interface |
| HAND | Height Above Nearest Drainage |
| HTE | High Temperature Events |
| HTTP | Hypertext Transfer Protocol |
| IW | Interferometric Wideswath |
| MODIS | Moderate Resolution Imaging Spectroradiometer |
| MSI | Multi-spectral Instrument |
| NDVI | Normalized Difference Vegetation Index |
| NIR | Near Infrared |
| OGC | Open Geospatial Consortium |
| OTB | ORFEO ToolBox |
| PSI | Persistent Scatterer Interferometry |
| PPP | Public Private Partnership |
| R&T | Research and Technology |
| S-1FS | Sentinel-1 Flood Service |
| S1TBX | Sentinel-1 toolbox |
| SAR | Synthetic Aperture Radar |
| SNAP | Sentinel Application Platform |
| SRTM | Shuttle Radar Topography Mission |
| SVM | Support Vector Machines |

| | |
|---|---|
| SWBD | SRTM Water Body Data |
| TFS | TerraSAR-X Flood Service |
| UNISTRA | Université de Strasbourg (University of Strasbourg) |
| VEAM | Vulnerable Element Activity Map |
| VNIR | Visible / NIR Infrared |
| WFS | Web Feature Service |
| WMS | Web Mapping Service |
| VHR | Very High Resolution |
| XML | Extensible Markup Language |

Intentionally blank

# Executive Summary

This document provides a report on the work carried out in Task 5.1 *Earth Observation*. It presents the technical specifications of the Earth Observation (EO) processing chains implemented and the description of the products provided within the HEIMDALL project.

The EO-based services make use of data from several optical and radar satellite sensors to provide large-scale crisis-related information in near-real time for natural disasters including fires, floods, and landslides in order to support decision makers and incident commanders during crisis situations, for preparation and in the aftermath.

The following EO-based processing chains are provided within HEIMDALL:

- Sentinel-1, TerraSAR-X, Sentinel-2 and Very High Resolution (VHR) flood processing chains
- Sentinel-2 burn scar mapping chain
- Fire severity processing chains
- Moderate Resolution Imaging Spectroradiometer (MODIS)-based hotspot service for wildfire detection
- Sentinel-2 landslide mapping chain
- Processing chain for updating landslide activity based on Sentinel-1 interferometric data

# 1 Introduction

The objectives of the HEIMDALL Earth Observation (EO) services are to provide reliable and high-quality satellite-based information as input for modelling and risk assessment as well as for supporting emergency response activities in case of fire, flood, and landslide events.

The EO services integrate satellite products from various optical and radar sensors in order to provide users large-scale crisis-related information in near-real time related to floods, forest fires and landslide events.

The following processing chains are used within HEIMDALL:

- Automatic Sentinel-1 [1] and TerraSAR-X [2] flood processing chains
- Automatic Sentinel-2 burn scar mapping chain [3]
- Automatic MODIS-based hotspot service for wildfire detection [4]
- Automatic Sentinel-2 flood processing chain [5, 6]
- VHR optical flood processing chain [5, 6]
- Sentinel-2 landslide mapping chain [6]
- Processing chain for updating landslide activity based on Sentinel-1 interferometric data [7]
- Processing chain for fire severity estimation [8]

The processing chains are separated from each other and provide reliable as well as high-quality products (flood masks, burn scars, fire hot spots, fire severity and information about landslide extents and landslide activity). These products, derived by these processing chains are provided by the German Aerospace Center (DLR), Université de Strasbourg (UNISTRA), and the Centre Tecnològic de Telecomunicacions de Catalunya (CTTC).

The data are automatically or semi-automatically processed by the partners and the final EO-based crisis information products are provided to the HEIMDALL Service Platform via a dedicated File Transfer Protocol (FTP) Server at DLR.

In comparison to D5.1 *EO Tools and Products – Specifications – Draft* a more detailed description of the module functionality and the EO-based processing chains is given. Further, Section 5.5 has been introduced with the aim of describing the processing chain for fire severity estimation based on optical remote sensing data.

The deliverable is organised in the following manner:

- Section 2 introduces the technical requirements of the Earth Observation services
- Section 3 describes the role of the module Earth Observation Products within the HEIMDALL overall architecture
- Section 4 describes the functionality of the module Earth Observation Products
- Section 5 presents the technical specifications of the Earth Observation processors and resulting products
- Finally, section 6 summarizes and concludes the document.

# 2 Earth Observation Technical Requirements

## *2.1 Interface Requirements*

### 2.1.1 **Hardware Interfaces**

The hardware setup utilized by the German Remote Sensing Data Center (DFD) of DLR is part of a distributed server infrastructure (Private Cloud). It is hosted by DLR and features, in total, 2070 CPU cores and 22.4 TB RAM, as well as one Petabyte storage.

UNISTRA has an internal server and distributed network that resembles a Private Cloud. Furthermore, it is leading a cloud development through the A2S programme and will implement its algorithms on this. This cloud is developed in conjunction with and uses UNISTRA HPC facilities.

CTTC hardware resources are internal to the institute headquarters and include an archive of a selected set of downloaded Sentinel images. Processing makes use of standard desktop PC and a central server unit.

### 2.1.2 **Software Interfaces**

The processing chains used for Sentinel-1 and TerraSAR-X flooded areas extraction, Sentinel-2 burnt area extraction and MODIS hotspots post-processing are each integrated in separate virtual machines (with VMware being used as hypervisor technology). All three productive machines are cloned in order to provide suitable development and testing instances. The operating system used on all virtual machines is Ubuntu Linux 16.04. The machines are interconnected by means of a local network.

The software utilized by DLR for the Sentinel-1/2 data is mainly the ESA ‘SNAP’ application, as well as ‘IDL/ENVI’ and Python. The former is used for the pre-processing of the input data, while the actual features extraction (burnt areas / flood masks) is done via ‘IDL’ (the only commercial component used) and Python. In case of Sentinel-2 data, ‘Sen2Core’ is used for additional pre-processing.

For landslides detection and monitoring, CTTC will use in-house processing chains and tools developed in C++ and ‘IDL/ENVI’ environment to process the Sentinel-1 data and generate the velocity and time series of deformation maps and the landslides map.

Regarding the MODIS data, the hotspot post-processing is done using the ‘Python’ programming language. The scripts mainly invoke the ‘GDAL/OGR’ - C/C++ - libraries via the ‘SWIG’-generated Python bindings. The purpose of the post-processing is the temporal/spatial filtering of the hotspot data and the enrichment with meta information (region of occurrence etc.).

UNISTRA will firstly implement its algorithms for Sentinel-2 and VHR optical water extraction and landslide mapping in an ArcGIS software interface that is currently operationally used in rapid mapping. The same initial software set-up is used for UNISTRA’s burn scar and fire severity mapping package. Python is extensively used within these procedures. Otherwise, a dedicated engineer will enable the implementation of UNISTRA’s algorithms onto the A2S platform.

### 2.1.3 **Communication Interfaces**

Regarding Sentinel-1/2 data, the processing system needs to contact the Copernicus Open Access Hub and download the required input data (via HTTP). After the processing steps are completed, the results are transferred to a dedicated file server through the ftp protocol, where they are harvested in order to be integrated into the final system.

The MODIS data is received at DLR-DFD, as is the case for the extraction of hotspots via the MOD14 algorithm. Therefore, the communication only comprises the data transfer to the processing machines via intranet. Analogous to the burnt areas, the final hotspot products are transferred to a machine with a running GeoServer instance for further distribution.

UNISTRA's processing system, regarding Sentinel-1/2 data, automatically contact the Amazon and/or Copernicus Open Access Hub and downloads the required input data (via HTTP). Otherwise, for demonstrators using non-Sentinel data UNISTRA sources the data manually making the imagery available to its in-house processing chains. The derived products are transferred internally to a dedicated machine. These sourcing methods are the same for flood, fire and landslide operations. UNISTRA distributes its results through the HEIMDALL platform via WFS.

CTTC downloads the required Sentinel-1 data from the Copernicus Open Access Hub (via HTTP) and makes the results available to the HEIMDALL platform via WFS.

## *2.2 Functional Technical Requirements*

### 2.2.1 **Short-Term Features**

No short-term features are defined within HEIMDALL concerning EO-tools and products.

### 2.2.2 **Mid-Term Features**

Table 2-1: Technical Requirement TR_DataEO_1

| | |
|---|---|
| Requirement ID: | TR_DataEO_1 |
| Related SR(s): | • Sys_DataEO_2 |
| **Description:**<br>The module Earth Observation Products shall be able to provide periodical information about burn scars based on Sentinel-2 and fire hot spots based on MODIS data in vector and raster format. | |
| Rational: The user can regularly get an overview of the active fires and of the burnt areas. | |
| Stimulus: Processors for burn scar and fire hot spot detection are triggered in case of the availability of relevant MODIS and Sentinel-2 acquisitions over an area of interest. | |
| Response: The system is able to visualize the burnt scars and active fire hot spots. | |
| Verification Criterion: Available burn scars and hot spots are on the GUI | |
| Notes: none | |

Table 2-2: Technical Requirement TR_DataEO_2

| | |
|---|---|
| Requirement ID: | TR_DataEO_2 |
| Related SR(s): | • Sys_DataEO_4 |
| **Description:**<br>The module Earth Observation Products shall be able to provide the flood layer produced by the project partners' automatic flood extraction systems in vector and raster format. | |

| |
|---|
| Rational: The user can get an overview of the flood extent. |
| Stimulus: A flood layer is derived by a project partners' automatic flood extraction system and uploaded onto the HEIMDALL system. |
| Response: The system is able to visualize the flood extent. |
| Verification Criterion: Proper displaying of flood layers in the GUI (full extent, resolution, zoom capacities, geometry, symbology, attributes…). |
| Notes: none |

Table 2-3: Technical Requirement TR_DataEO_4

| | |
|---|---|
| Requirement ID: | TR_DataEO_4 |
| Related SR(s): | • Sys_DataEO_5 |
| **Description:**<br>The module Earth Observation Products shall be able to provide information on the landslide extent based on Sentinel-2 data in vector and raster format as well as information about the movement of landslides based on Sentinel-1 data | |
| Rational: The user can get an overview of the landslide extent and movement. | |
| Stimulus: Information about the landslide extent and movement is derived by project partners' landslide detection and monitoring systems and uploaded onto the HEIMDALL system. | |
| Response: The system is able to visualize the information about the landslides. | |
| Verification Criterion: Proper displaying of the layers related to information about the landslides (full extent, resolution, zoom capacities, geometry, symbology, attributes…). | |
| Notes: none | |

### 2.2.3 **Long-Term Features**

Table 2-4: Technical Requirement TR_DataEO_3

| | |
|---|---|
| Requirement ID: | TR_DataEO_3 |
| Related SR(s): | • Sys_DataEO_5 |
| **Description:**<br>The module Earth Observation Products shall be able to allow the user to download the extracted crisis layers (flood masks, burn scars, fire hotspots, landslide-affected areas, etc.) in vector and raster format and its metadata. | |
| Rational: The user can download and integrate the extracted crisis layers in its own database and interface. | |
| Stimulus: The module is triggered by the user by downloading the crisis layers. | |

| |
|---|
| Response: Download of the crisis layers. |
| Verification Criterion: Proper download of the crisis layers and metadata (full extent, resolution, attributes, format). |
| Notes: none |

## *2.3 Other Requirements*

### 2.3.1 **Short-Term Requirements**

No non-functional short-term requirements have been identified.

### 2.3.2 **Mid-Term Requirements**

No non-functional mid-term requirements have been identified.

### 2.3.3 **Long-Term Requirements**

No non-functional long-term requirements have been identified.

# 3 Reference Architecture

This sub-section illustrates the HEIMDALL overall architecture highlighting the module Earth Observation Products addressed in the current technical specification. The module Earth Observation Products is part of the system inputs to the HEIMDALL Service Platform. Inputs to this module are various satellite data which are systematically acquired or are tasked on-demand over an area of interest. The satellite data used in HEIMDALL are Synthetic Aperture Radar (SAR) (TerraSAR-X and Sentinel-1) or optical (MODIS, Sentinel-2, and Very High Resolution e.g. Pléiades, SPOT-7) data.

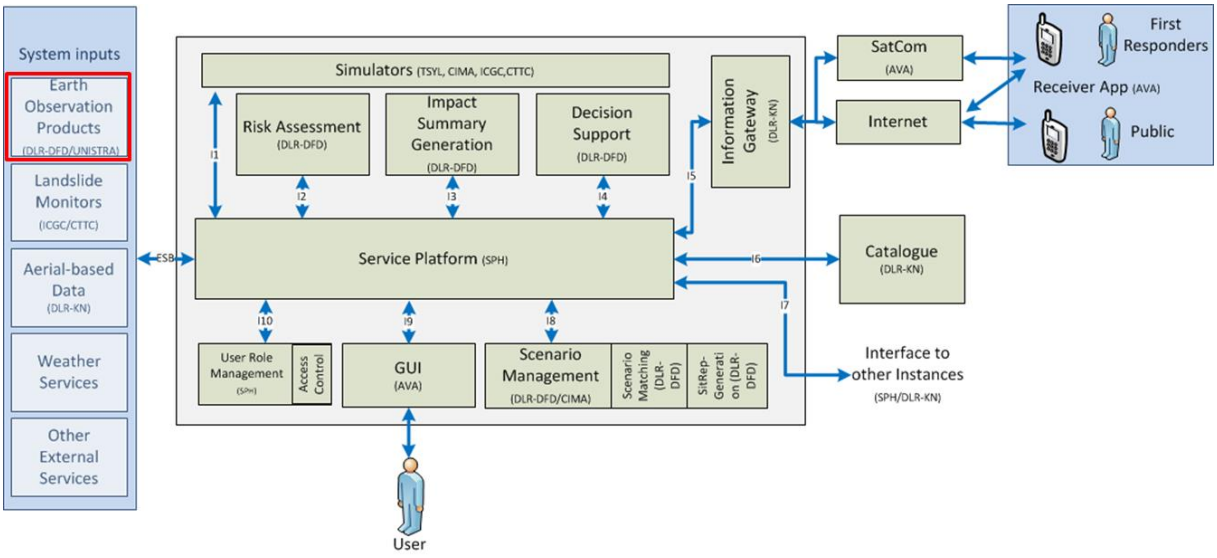


Figure 3-1: HEIMDALL architecture

Outputs of the module are several crisis products based on multi-sensor Earth Observation data generated in the context of the natural disasters flooding, fires, and landslides. This includes the following products: flood masks, burn scars, fire hot spots, information on fire severity, masks showing the extent of abrupt landslides as well as information about the velocities of slow-moving landslide events.

The products will be provided as vector and/or raster files to the Service Platform via Web Feature Services (WFS) or Web Mapping Services (WMS) and will be derived by the following semi-automatic and automatic services:

- Automatic Sentinel-1 and TerraSAR-X flood processing chains
- Automatic Sentinel-2 burn scar mapping chain
- Automatic MODIS-based hotspot service for wildfire detection
- Automatic Sentinel-2 flood processing chain
- Processing chain for fire severity estimation
- VHR optical flood processing chain
- Sentinel-2 landslide mapping chain
- Processing chain for updating landslide activity based on Sentinel-1 interferometric data.

# 4 Module Functionality

This section describes the functionality of the module Earth Observation Products, which delivers several product outputs to the HEIMDALL Service Platform based on processing chains.

The different processing chains related to floods, forest fires and landslide events follow the generic structure visualized in Figure 4.1 and are either automatic or semi-automatic.

In the case of a disaster the processing chains can be triggered by the user by sending a request of Earth Observation-based products to the respective operators of the processing chains via the HEIMDALL Service Platform (Figure 4.2). Based on the parameters sent by the user (e.g. disaster type and date, area of interest, etc.) satellite data are tasked. The acquired optical or radar satellite acquisitions are ingested in the processing chains. The data are pre-processed and analysed using semi-automatic or automatic thematic processors for the derivation of the relevant crisis information related to floods, forest fires, and landslide events. Auxiliary data sets such as land cover or topographic information are used for improving the pre-processing and classification steps. Optional post-processing is performed to improve the initial classification results. The extracted EO-based products are finally disseminated as WMS or WFS in GeoTIFF/ESRI Shapefile format to the HEIMDALL Service Platform via FTP.

Technical specifications to the respective processing chains are provided in Chapter 5.

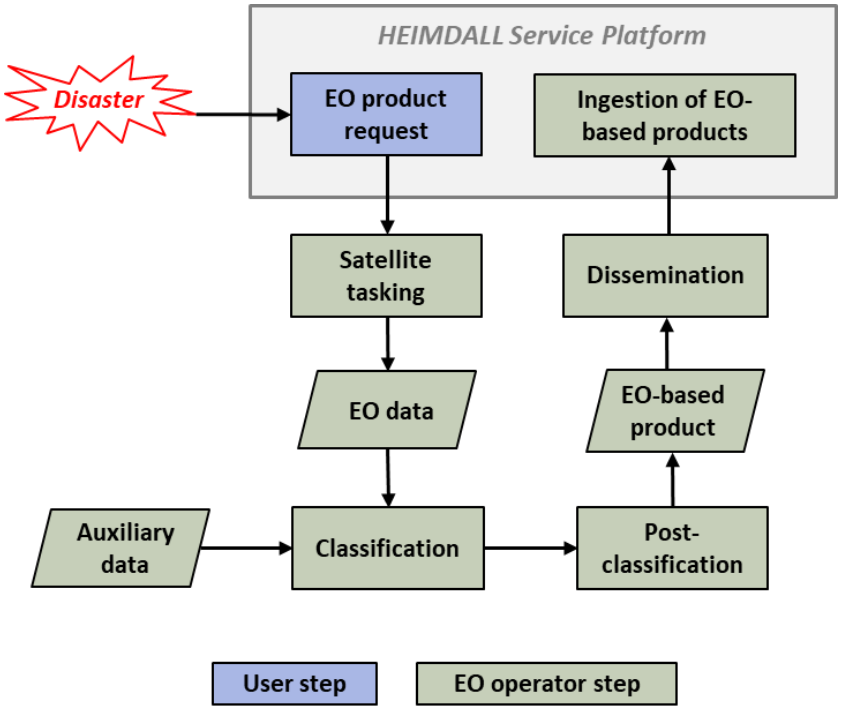


Figure 4-1: Generic workflow of the processing chains of the module Earth Observation Products

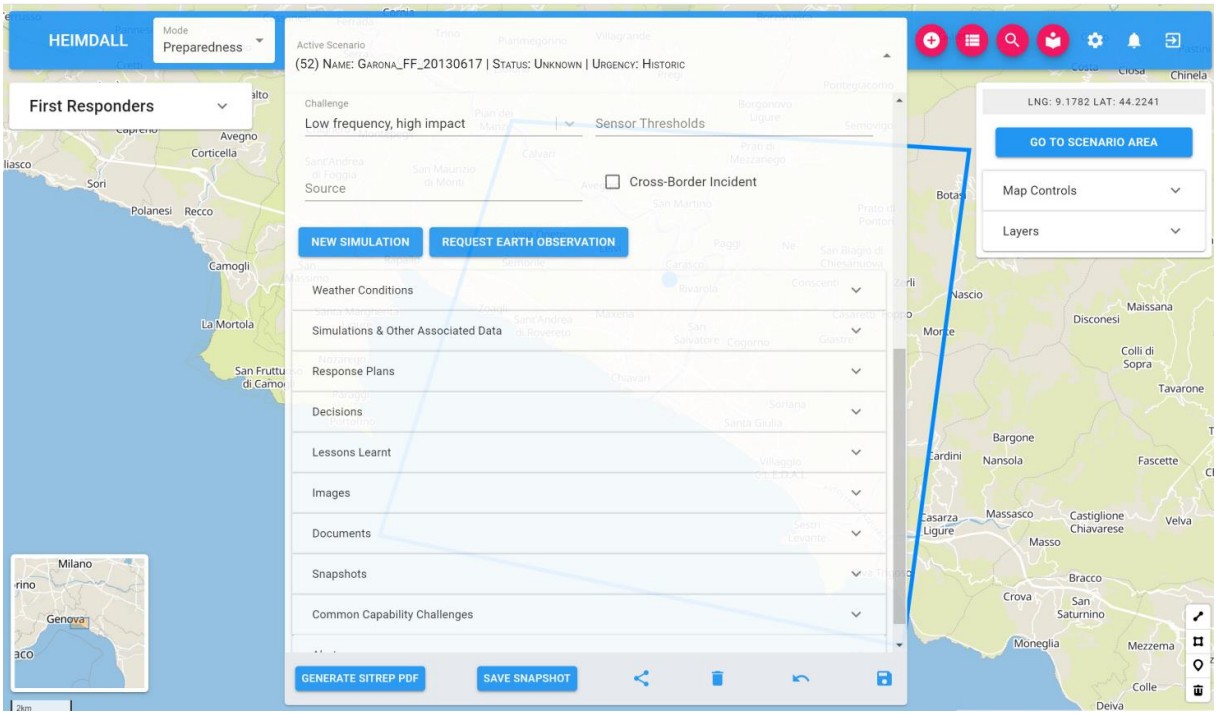


Figure 4-2: Screenshot of the template for requesting EO-based products via the HEIMDALL GUI

# 5 Technical Specification of the Earth Observation Processing Chains

Within this chapter the technical specifications of the Earth Observation-based processing chains provided within HEIMDALL are described. Table 5-1 gives an overview about the main characteristics of the respective processing chains, which are specified in more detail in the following sub-chapters.

Table 5-1: Overview about the main characteristics of the EO-based processing chains

| Processing chain | Input | Product | Short description | Format | Dissemination |
|---|---|---|---|---|---|
| Sentinel-1 flood processing chain | Sentinel-1 data | Flood extent | Flood binary mask (with permanent water areas excluded) | GeoTIFF, ESRI Shapefile | WMS, WFS |
| TerraSAR-X flood processing chain | TerraSAR -X data | Flood extent | Flood binary mask (with permanent water areas excluded) | GeoTIFF, ESRI Shapefile | WMS, WFS |
| Sentinel-2 flood processing chain | Sentinel-2 data | Flood extent | Flood binary mask (with permanent water areas excluded) | GeoTIFF, ESRI Shapefile | WMS, WFS |
| VHR optical flood processing chain | VHR optical data | Flood extent | Flood binary mask (with permanent water areas excluded) | GeoTIFF, ESRI Shapefile | WMS, WFS |
| Sentinel-2 burn scar mapping chain | Sentinel-2 data | Burn scar | Burnt areas binary mask (extent) | GeoTIFF, ESRI Shapefile | WMS, WFS |
| SWIR based fire severity processing chain (Sentinel-2 like data) | Sentinel-2 like optical data (with SWIR) | Fire severity | Classification of the fire severity level within the burnt areas (up to 3 classes) | GeoTIFF, ESRI Shapefile | WMS, WFS |
| Fire severity processing chain based on data without SWIR (Pléiades-HR like data) | Pléiades-HR like optical data (without SWIR) | Fire severity | Classification of the fire severity level within the burnt areas (up to 3 classes) | GeoTIFF, ESRI Shapefile | WMS, WFS |
| MODIS-based hotspot service for wildfire detection | MODIS data | Fire hot spots | Thermal anomaly locations enhanced with meta data | ESRI Shapefile | WFS |
| Sentinel-2 landslide mapping chain | Sentinel-2 data | Landslide extent | Binary mask of abrupt landslide affected areas | GeoTIFF, ESRI Shapefile | WMS, WFS |
| Sentinel-1 landslide activity mapping service | Sentinel-1 data | Information about landslides | Velocity of slow-moving landslides | ESRI Shapefile | WFS |

## *5.1 TerraSAR-X and Sentinel-1 Flood Service*

### 5.1.1 **SAR-based flood detection**

Radar satellite remote sensing has proven to provide essential large-scale information on flood situations. The near-real time provision of detailed information on inundation extent and its spatio-temporal evolution is essential for supporting flood relief efforts. Due to the independence of the microwave signal to weather and illumination, radar based methods are particularly suitable for a systematic flood monitoring strategy [2].

The detectability of water in SAR imagery is controlled by the contrast between water areas and the surrounding land, which is highly influenced by surface roughness characteristics, and the system-specific parameters wavelength, incidence angle of the radar beam and polarization.

Smooth open water areas can be relatively easily detected in the radar data. A flat water surface acts as a specular reflector which scatters the radar energy away from the sensor. This causes relatively dark pixels in radar data which contrast with non-water areas. With decreasing system wavelength the sensitivity of a smooth water surface to diffuse scattering increases. However, as the number of possible objects on the land that might appear smooth and have a similar backscatter as water is reduced at longer wavelengths, a higher contrast ratio between water and the land areas occurs at higher system frequencies. Consequently, water monitoring using X-band SAR is more suitable than using longer wavelengths e.g. in the C- and L-band domain [9].

Also the type of polarization plays an important role in detecting open water bodies, which describes the restriction of electromagnetic waves to a single plane perpendicular to the direction of propagation of the SAR signal. Polarimetric SAR systems transmit either in a horizontal (H) or vertical (V) plane, which also can be received horizontally or vertically. Thus, there can be two possibilities of like- (HH, VV) and cross-polarization (HV, VH). Generally, HH polarization provides the best discrimination between water and non-water terrain [e.g. 10]. This is caused by a low scattering of the horizontal component of the signal from the smooth open water surface [9].

Since the launch of the high-resolution SAR satellite systems TerraSAR-X, RADARSAT-2 and the COSMO-SkyMed constellation, a small number of automatic image processing algorithms have been developed to derive open flood surfaces from SAR data [9-12]. These algorithms have in common that they make use of automatic thresholding algorithms for the initialization of the classification process.

Even if relevant crisis information can be extracted automatically, in most cases a certain amount of user interaction is needed for data pre-processing, the collection and adaptation of auxiliary data useful for classification refinement as well as the preparation and dissemination of the crisis information to end users. Only few operational SAR-based flood services exist to date: An on-demand TerraSAR-X Flood Service consisting of a fully automated processing chain geared towards near-real-time flood detection is presented in [2]. This TerraSAR-X Flood Service has been adapted to the systematic data stream of the Sentinel-1 mission [1], operated by the European Space Agency (ESA) in the frame of the European Union’s Copernicus Programme.

### 5.1.2 **TerraSAR-X and Sentinel-1**

TerraSAR-X is a German on-demand Earth-observation satellite, operated by DLR under a so-called Public-Private Partnership (PPP) between DLR and Airbus Defence and Space. Its primary payload is an X-band radar sensor with a range of different modes of operation, allowing it to record images with different swath widths, resolutions and polarisations (VV,

VV, VH, HV). TerraSAR-X and its twin TanDEM-X have been launched in 2007 and 2010, respectively.

Future data takes may be directly ordered by users using several acquisition modes listed in table 5.2.

Table 5-2:TerraSAR-X acquisition modes [15]

| Mode | Coverage Azimuth x Range (km2) | Resolution Class (m) |
|---|---|---|
| ScanSAR Wide (SCW) | 200 x (194–266) | 40 |
| ScanSAR (SC) | 150 x 100 | 18 |
| StripMap (SM) | 50 x 30 | 3 |
| Spotlight (SL) | 10 x 10 | 1.7 - 3.5 |
| High-Resolution Spotlight (HS) | 5 x 10 | 1.4 - 3.5 |
| 300 MHz High-Resolution Spotlight (HS 300) | 5 x (5-10) | 1.1 - 1.8 |
| Staring Spotlight (ST) | (2.5 – 2.8) x ~ 6 | 0.24 azimuth, 1.0 range |

Depending on the repeat cycle of TerraSAR-X of 11 days, on the selected acquisition mode and on the geographic location of the disaster area a revisit time of 1-5 days can be achieved.

The Sentinel-1 mission is operated by ESA in the frame of the European Union's Copernicus Programme and consists of two systematically acquiring satellite sensors, Sentinel-1A (launched in 2014) and Sentinel-1B (launched in 2016), with a repeat cycle of 6 days for the final constellation. Sentinel-1A and B are equipped with a C-Band SAR payload (at 5.405 GHz). Over land masses, the interferometric wide swath (IW) mode is used by default, acquiring SAR data with VV or VV/VH polarization at a spatial resolution of ~20m. The mission is based on a pre-defined conflict-free observation scenario making optimum use of the SAR duty cycle with respect to the technical constraints of the system [16]. This is a major advantage for the implementation of fully automated processing chains as the time consuming step of tasking satellite data can be omitted.

### 5.1.3 **TerraSAR-X and Sentinel-1 flood processing chain**

**TerraSAR-X flood processing chain**

For the provision of TerraSAR-X based flood masks within HEIMDALL DLR's on-demand TerraSAR-X-Flood Service (TFS) developed by [2] is used, which consists of a fully automated processing chain geared towards near-real time pixel-based flood detection.

The fully automated processing chain includes the download and pre-processing of TerraSAR-X data, computation and adaption of global auxiliary data (reference water masks, digital elevation models, topographic slope information), unsupervised class initialization, post-classification refinement and dissemination of the flood masks. An overview about the workflow is presented in Figure 5.1.

For the unsupervised initialization of the flood processor a parametric tile-based thresholding procedure is applied. This approach was originally developed by [11] to automatically detect the inundation extent in SAR amplitude data with even small a priori probabilities of the

class-conditional densities of the class flood within the histogram of the entire SAR scene in a time-efficient manner. This method was enhanced in robustness in [2].

The initialization consists of the following processing steps: image tiling, tile selection and sub-histogram based thresholding of a small number of tiles of the entire SAR image selected according to the probability of the tiles to contain a bi-modal mixture distribution of the classes to be separated (classes flood and non-flood).

The tiling and tile selection is based on statistical hierarchical relations between parent and child objects in a bi-level quadtree structure of the data. The Kittler and Illingworth minimum error thresholding approach [17] is used to derive local threshold values using a cost function which is based on modelling the sub-histograms of each selected tile as bi-modal Gaussian mixture distributions.

One global threshold is obtained by computing the arithmetic mean of the local thresholds. A fuzzy logic-based algorithm is used for post-classifying the initial labelling result derived by the application of the global threshold to image the SAR data. The fuzzy set is built using the following four elements: SAR backscatter, digital elevation and slope information as well as the size of flood surfaces. The fuzzy threshold values of each element are either determined according to statistical computations or are set empirically. The corresponding fuzzy elements are combined into one composite fuzzy set by computing the average of the membership degrees of each pixel. The flood mask is created through a threshold defuzzification step, which transforms each image element with a membership degree >0.6 into a crisp value, i.e., a discrete label.

To differentiate between flooded areas and standing water bodies, the classification result is compared to a global reference water mask (SRTM Water Body Data [18] or MOD44W data [19]).

The final flood and reference water masks and satellite footprints are stored in a database in raster and vector format, respectively. The processing is based on a framework of Web Processing Services standard-compliant to the Open Geospatial Consortium (OGC).

Since TerraSAR-X is acquiring data non-systematically, this flood mapping service needs to be activated on-demand in case of emergency situations by programming dedicated satellite acquisitions over flood-affected regions. More details on the methodology of the TFS can be found in [2].

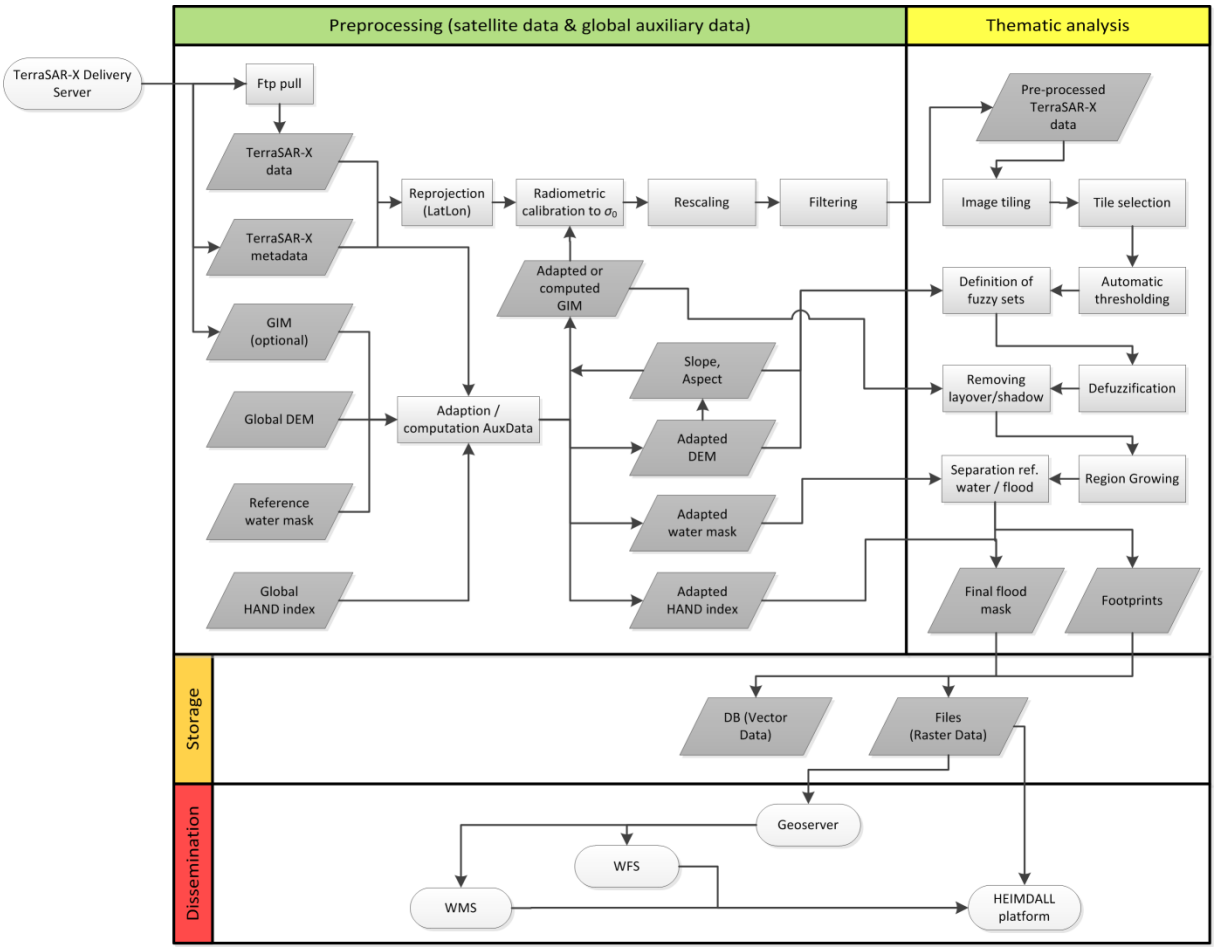


Figure 5-1: Workflow of DLR's TerraSAR-X Flood Service (TFS) [2, modified]

### Sentinel-1 flood processing chain

The methodology of the TerraSAR-X Flood service was adapted to Sentinel-1 radar data by [1]. This Sentinel-1 Flood Service (S-1FS) is used in HEIMDALL for systematic flood monitoring. The workflow of the Sentinel-1-based processing chain, as outlined in Figure 5-2, is composed of the following main elements: (a) automatic data ingestion through a Python-based script, which routinely queries the ESA Sentinel Data Hub for new acquisitions matching user-defined criteria and downloads them, (b) geometric correction and radiometric calibration using the graph processing tool (GPT) of the ESA's Sentinel Application Platform (SNAP), (c) initial classification using automatic thresholding, (d) fuzzy-logic-based classification refinement, (e) final classification including auxiliary data, and (f) dissemination of the results.

The service is targeted towards the processing of Sentinel-1 ground range detected (GRD) data acquired in IW mode, which are routinely being acquired over several land masses. Level-1 GRD products consist of focused SAR data that have been detected, multi-looked, and projected to ground range using an Earth ellipsoid model. In addition to satellite data, the processor makes use of several auxiliary data sets: Shuttle Radar Topography Mission (SRTM) 1 arc second data are used for the Range Doppler terrain correction and radiometric calibration of Sentinel-1 data.

The processing chain is activated through a Python-script, which routinely polls the ESA Sentinel Data Hub for new acquisitions matching user-defined criteria. Using these criteria, for example, the time frame or geographical location of suitable Sentinel-1 acquisitions can be specified. Once corresponding scenes are found, these are downloaded to the local file system and the thematic processor is executed. After unzipping the data, the folder structure

is searched for files relevant for the further processing, namely Sentinel-1 data in GeoTIFF-format and Extensible Markup Language (XML) metadata used for radiometric calibration. During the pre-processing step, a Range-Doppler terrain correction of Sentinel-1 data and radiometric calibration to sigma naught (dB) are performed using the GPT of ESA's Sentinel Application Platform (SNAP). For the automatic classification of the flood extent the automatic tile-based thresholding and fuzzy-logic-based post-classification refinement step as described in [2] is used.

Besides fuzzy-logic-based classification refinement, the thematic accuracy of the processor is further enhanced through the integration of the 'Height above nearest drainage' (HAND) index [20], which helps to reduce water-lookalikes depending on the hydrologic–topographic setting. The HAND index has been calculated near-globally based on elevation and drainage direction information provided by the Hydrosheds mapping product [21]. Based on the HAND index, a binary exclusion mask (termed 'HAND-EM') has been calculated to separate flood-prone from non-flood prone areas. Both binary classes are determined using an appropriate threshold value. The exclusion mask based on the HAND-index is applied to mask out potential misclassifications in all areas with a HAND-index value of ≥15 m above the drainage network.

The processing results are stored as GeoTIFF raster files as well as vector files. These results are transferred to a dedicated file server, where they can be harvested in order to be incorporated into the final system.

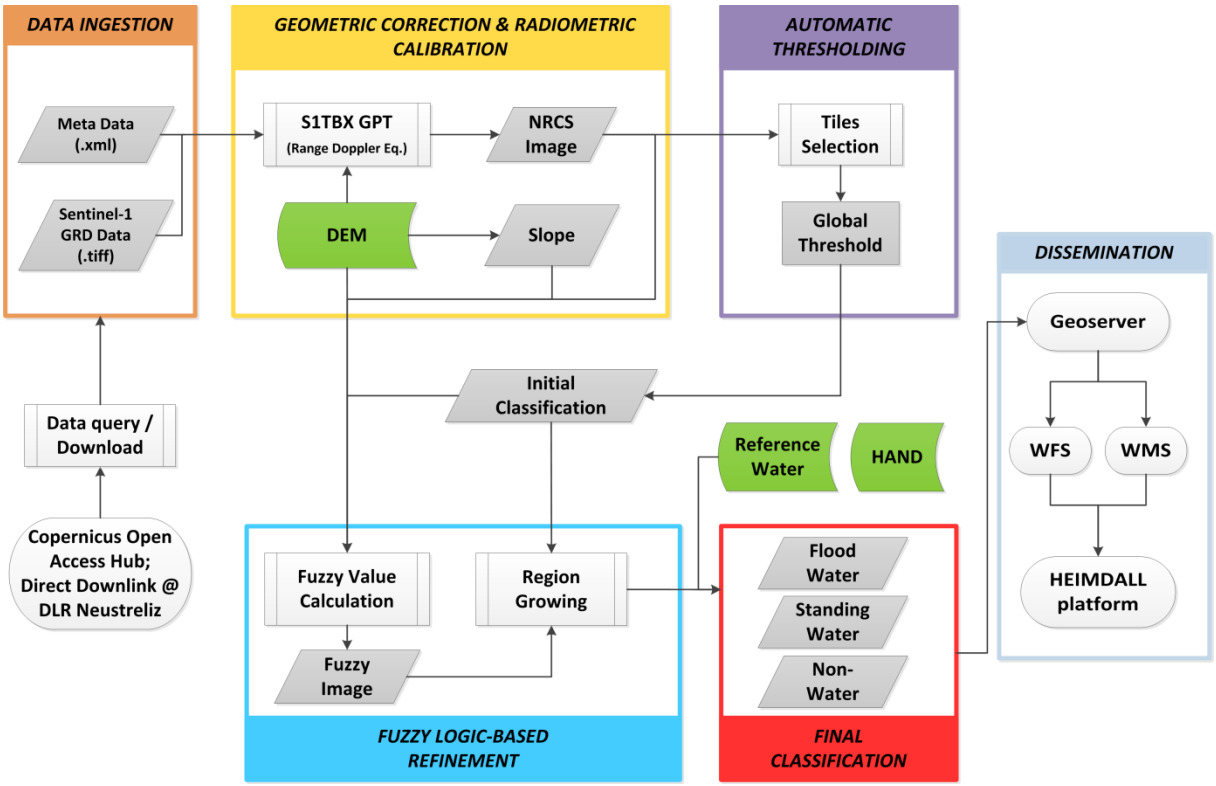


Figure 5-2: Workflow of DLR's Sentinel-1 Flood Service (S-1FS) [1, modified]

## 5.1.4 **Products**

The products derived by the TerraSAR-X and Sentinel-1 flood processing chains are flood masks which give an overview of the open water extent of a flood situation at a certain time.

The spatial resolution and coverage of the TerraSAR-X flood masks correspond to the spatial resolution of the acquisition mode chosen for observing the affected areas: the higher the spatial resolution the lower the coverage of the satellite footprint. The highest spatial

resolution is related to the Staring Spotlight mode (resolution: 0.24 m, coverage: ~2.5*6 km), the lowest resolution to the Wide ScanSAR mode (resolution: 40 m, coverage: ~200*194-266 km).

The spatial resolution of the Sentinel-1 flood masks is ~20 m corresponding to the spatial resolution of the Interferometric Wideswath (IW) mode, which is the standard mode of the Sentinel-1 mission over land surfaces. Binary flood masks as well as masks showing permanent water surface based on SRTM Water Body Data (SWBD, 30 m spatial resolution) are provided as part of HEIMDALL in both raster (GeoTIFF) and vector (ESRI Shapefile) format to users.

The produced and subsequently accumulated vector Sentinel-1 and TerraSAR-X-based flood masks X are then transferred to a dedicated file server in the format of ESRI Shapefiles.

The flood services contain all recent detections for the areas of interest. They are updated as soon as new data becomes available. In this case, also a notification is generated by the system to inform applicable stakeholders about the updated status using a publish/subscribe mechanism. The WebHooks technology is utilized for implementing this functionality. This mechanism is used with all services published by DLR as part of HEIMDALL.

## *5.2 VHR optical and Sentinel-2 flood processing chains*

### 5.2.1 Optical data-based flood detection

UNISTRA established an automatic water surface extraction procedure in HEIMDALL that ingests optical data and outputs a water layer.

In this context, UNISTRA worked on two different approaches for flood mapping from optical data. One branch focused on new methods involving complex machine learning workflows, which often involve the use of samples, and another using robust thresholding methods using simple band values and sampling. UNISTRA worked on automatic sampling methods using world-wide flood databases to enable a fully automated processing chain.

**Supervised machine learning techniques**

In the search for easily implemented machine learning techniques, as already stated in the ESA-funded research project ASAPTERRA [6], much of the work to date performed relies on specific extraction techniques, including pixel-based, region-based and knowledge-based methods [22-24]. Pixel-based methods are the most commonly used spectral information to classify remote sensing imagery. In complex situations, it is sometimes difficult to extract water bodies on a pixel by pixel basis because the algorithm does not bring the necessary spatial information to interpret the image [25-26]. Furthermore, in the past few decades, object-based algorithms have been developed exploiting spatial information in the procedure but the desired results are not always obtainable. Most of these methods used alone do not provide reliable accuracy in flood situations. Some studies and work within ASAPTERRA have found that Support Vector Machines (SVM) and Artificial Neural Networks (ANN) perform better than traditional methods [24-27]. Work within ASAPTERRA by UNISTRA led to a preference for SVM due to high accuracy and ease of implementation. Below, SVMs are briefly described.

Optical data are often affected by clouds, haze and shadows and it is important to take these into account to reduce misclassification, especially in the case of HR or VHR images. Furthermore, the detection of water areas also relies on the sensitivity of the sensor and its spatial resolution. For this reason, it is strongly recommended to choose wisely the data set of images on which the work is performed to develop a tool. The aim of UNISTRA was to extract water and also eliminate non-water features which have similar spectral values. Such misclassification can be reduced by choosing smartly and precisely an adequate number of samples for the training of the classifiers.

***Support Vector Machines (SVM)*** are a powerful machine learning procedure created by [28] and are useful because of their exploitability in a large range of applications [29, 30]. The power of SVMs relies on the kernel function which can adapt its dimension function compared to the mapping input [31]. In addition, the kernel can adapt itself into a matrix kernel instead of high dimensional space if the classes are not separable in the input space.

**Robust thresholding techniques**

The other approach as already stated is to use robust thresholding methods to derive a water mask. Given the context of rapid mapping it is necessary that the work flow runs quickly, involving not too much image processing and where possible automating the operation. This is of course the same in systematic flood mapping tools except in this case, there is less emphasis on speed of execution.

The work conducted in [6] confirmed the large variation in water surface radiometric characteristics and, hence, the need to capture this variability in a classification workflow. Another issue encountered was the need to derive samples to help the various supervised classification procedures to produce an adequate water mask, of course taking the radiometric variability of the data into account. Of course, an essential requirement is to establish the optimal input material to be classified and the classification method itself. The input material, a combination of simple satellite sensor bands, water oriented indices, plus exogenous data, will depend to a large extent on the composition of the satellite images available and exogenous databases that are available.

UNISTRA chose the database to be integrated into its sample selection procedure and has developed an initial automated processing chain covering all phases:

- Satellite data access and selection
- Satellite data input
- Sample selection and generation
- Signature creation
- Classification

An automatic Sentinel-2 data reading module that is capable of inputting the satellite images into the process has been developed. Figure 5-3 describes the status of the water mapping chain at the start of the automatic sample generation phase. UNISTRA has worked on automating the procedure, including automatic sampling, the choice of the input imagery layers (bands, etc.) and the classification method to implement.

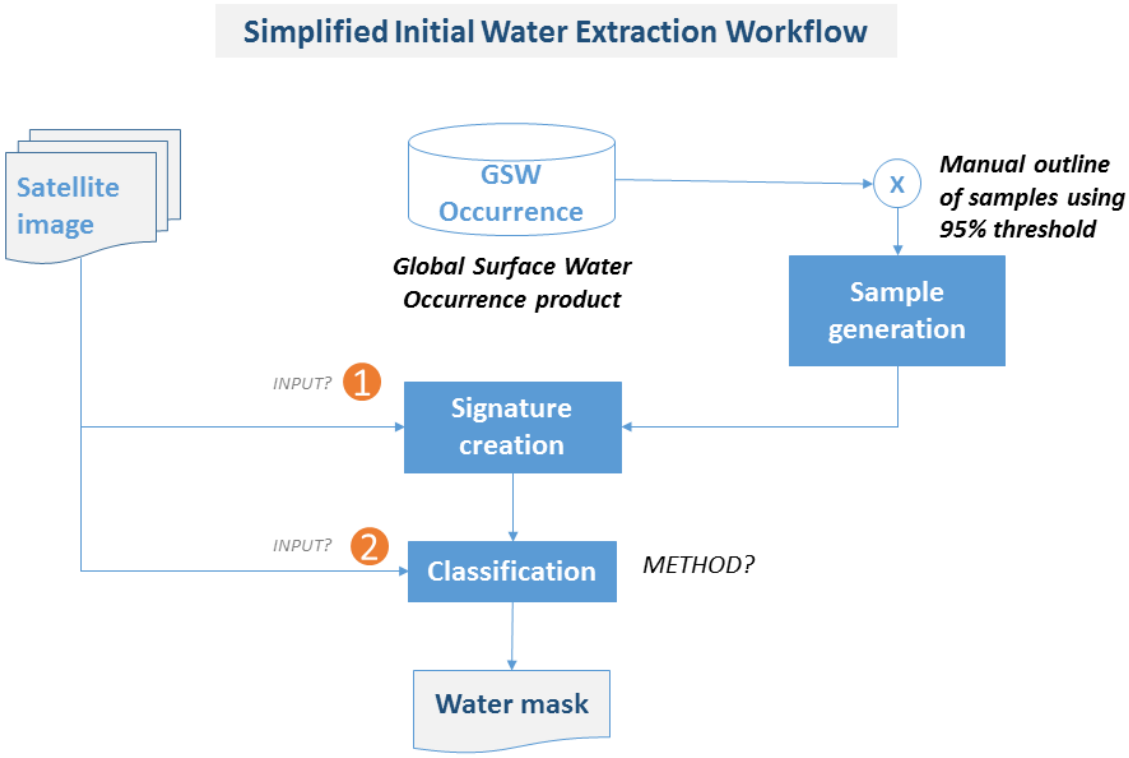


Figure 5-3: Initial status of the optical data-based flood detection workflow previous to the HEIMDALL work

One of the main hurdles is to select and automatically extract samples. Part of this work is to select an optimal database for selecting samples. Below the database selection procedure is outlined.

**Selecting a database for sample selection**

Whatever approach is applied, machine learning or simple thresholding, the question of how to obtain samples to feed into the classification procedure is an essential issue. To streamline the selection of samples, UNISTRA has extensively analysed water body databases that could be a major input into this process. Within a CNES supported R&T contract [5] UNISTRA statistically analysed the databases mentioned in Table 5-3. Too many inconsistencies within the databases were observed between the case study areas and hence a more qualitative but broader assessment was performed. It must be stated that only free to use databases are considered with the target of choosing a source that:

- is homogeneous,
- has worldwide coverage,
- is particularly good for sampling (trustworthy over permanent water bodies).

Table 5-3: List of global databases containing water classifications analysed within [5]

| No. | Data base |
|---|---|
| 1 | ESA Globcover 2009 |
| **2** | ESRI v9 |
| 3 | FROM_GLC |
| **4** | Global 3-second Water Body Map (G3WBM) |

| | |
|---|---|
| 5 | Global Inland Water |
| **6** | Global Lakes and Wetlands Database |
| 7 | Global Land Cover Share Database (2013) |
| **8** | Glowabo |
| 9 | ISCGM (GLCNMO) |
| **10** | MODIS Water Mask |
| 11 | OSM |
| **12** | Pekel 1% |
| 13 | Pekel 95% |
| **14** | Sheng |
| 15 | SWBD |
| **16** | USGS Global Land Cover |
| 17 | Vmap0 |

The qualitative classification employs a series of criteria chosen in order to analyse and class the databases and whether they might be good for selecting samples or validation of floods (Table 5-4). In this case, only sampling selection is analysed.

Table 5-4: Qualitative criteria used to classify the water databases

| Criteria | Description | Detail |
|---|---|---|
| **1** | Reliability / validation | Is the methodology documented and has it been validated? |
| **2** | Age | Since when it has been updated? |
| **3** | Genealogy | Depth/richness of database used to derive the final data |
| **4** | Update | Update frequency |
| **5** | Accuracy | Statistical evaluation of the database of test sites.<br>Only accuracy level is used for the sampling phase. |
| **6** | Resolution | Spatial resolution of the database |

A value range between 1 and 3 is given to each criteria and a weighting is calculated as it is considered that the selected criteria are not all equal, some being more important than others. The weighting of each criterion is described in Table 5-5. Criteria 5 is treated differently as the level of accuracy and the level of detection are transposed into the 1-3 interval. With 1 being applied to values below 50%, the remaining values [50%-100%] are stretched in order to obtain a dynamic of significant values above 50% accuracy between 1 and 3.

Table 5-5: Value classes and weightings are allocated to each criterion to analyse the databases

| | **Criteria** | | | | | |
|---|---|---|---|---|---|---|
| | **1** | **2** | **3** | **4** | **5** | **6** |
| | Reliability | Age | Genealogy | Update | Accuracy | Resolution |
| **Weighting** | 4 | 2 | 1 | 3 | 6 | 5 |

Points are allocated to each criterion following the criteria outlined in the tables below:

Table 5-6: Classes for criteria 1

| **Reliability** | **Points** |
|---|---|
| Validated & documented | 3 |
| Documented or validated | 2 |
| No information | 1 |

Table 5-7: Classes for criteria 2

| **Age** | **Points** |
|---|---|
| > 2010 | 3 |
| 2000 - 2010 | 2 |
| < 2000 | 1 |

Table 5-8: Classes for criteria 3

| **Genealogy** | **Points** |
|---|---|
| Global | |
| >=10 years | 3 |
| 5-10 years | 2 |
| <5 years | 1 |

Table 5-9: Classes for criteria 4

| **Update frequency** | **Points** |
|---|---|
| Annual | 3 |
| 1-5 years | 2 |
| >5 years | 1 |

Table 5-10: Classes for criteria 5

| **Accuracy** | **Points** |
|---|---|
| Level of accuracy $j$ | $j \in [0;50] \rightarrow 1$<br>$j \in [50;100] \rightarrow \frac{2}{50} \times (j-50)+1$ |
| Level of detection $d$ | $\frac{2}{100} \times d + 1$ |

Table 5-11: Classes for criteria 6

| Resolution / Scale | Points |
|---|---|
| 1m - 30m / 1:1 – 1:60 000 | 3 |
| 31m - 90m / 1:60 000 – 1:180 000 | 2 |
| 91m - 1km / 1:180 000 – 1:2 000 000 | 1 |

The spatial precision of a database is expressed by a distance and a scale, which are mathematically related: divide the denominator of the map scale by 1000 to get the detectable size in meters. The resolution is one half of this amount, or the equivalent of 0.5 mm on the map [32].

In the following Table 5-12, which is adapted from [5], the 17 databases are evaluated according to the 6 criteria already described and ranked according to appropriateness in the task of being applied globally for extracting classification samples. Quite clearly the Global Surface Water Occurrence database at 95% threshold is the best database for this task.

Table 5-12: Ranking of global, water surface containing, databases with respect to their pertinence in selecting samples for flood-time water body mapping

| Ranking | Database name | Criteria 1 | Criteria 2 | Criteria 3 | Criteria 4 | Criteria 5 | Criteria 6 | Result |
|---|---|---|---|---|---|---|---|---|
| | | Producer's accuracy | Age | Genealogy | Update frequency | Level of accuracy (Alsace) | Resolution | |
| | **Weighting** | 4 | 2 | 1 | 3 | 6 | 5 | |
| | **Classes** | 1-3 | 1-3 | 1-3 | 1-3 | 1-3 | 1-3 | |
| 1 | Global Surface Water Occurrence 95% | 3 | 3 | 3 | 1 | 3 | 3 | 57.0 |
| 2 | Global Surface Water Occurrence 1% | 3 | 3 | 3 | 1 | 2.7 | 3 | 55.2 |
| 3 | Global 3-second Water Body Map (G3WBM) | 3 | 3 | 3 | 2 | 2.7 | 2 | 53.2 |
| 4 | Global Inland Water | 3 | 2 | 2 | 1 | 2.8 | 3 | 52.8 |
| 5 | FROM - GLC | 3 | 2 | 3 | 2 | 2 | 3 | 52.0 |
| 6 | SWBD | 2 | 2 | 1 | 2 | 2.8 | 3 | 50.8 |
| 7 | Sheng | 1 | 3 | 2 | 2 | 2.9 | 3 | 50.4 |
| 8 | OSM | 1 | 2 | 3 | 3 | 2.7 | 1 | 41.2 |
| 9 | ESA_Globcover | 3 | 2 | 1 | 2 | 2.1 | 1 | 40.6 |
| 10 | ISCGM (GLCNMO) | 2 | 2 | 3 | 2 | 2.3 | 1 | 39.8 |
| 11 | ESRI_v9 | 2 | 1 | 1 | 3 | 1.4 | 2 | 38.4 |
| 12 | Glowabo | 2 | 3 | 3 | 3 | 1 | 1 | 37.0 |
| 13 | MODIS Water Mask | 2 | 2 | 1 | 1 | 2.1 | 1 | 33.6 |
| 14 | Global Land Cover Share Database (2013) | 3 | 3 | 1 | 1 | 1 | 1 | 33.0 |
| 15 | Vmap0 | 1 | 1 | 1 | 3 | 1 | 1 | 27.0 |
| 16 | USGS Global Land Cover Land Use/Land Cover | 1 | 2 | 2 | 1 | 1 | 1 | 24.0 |
| 17 | Global Lakes and Wetlands Database | 1 | 1 | 1 | 1 | 1 | 1 | 21.0 |
| | **MAXIMUM VALUE** | 3 | 3 | 3 | 3 | 3 | 3 | 63.0 |

The selected database, the Global Surface Water Occurrence map, is the result of work by scientists within the European Commission's Joint Research Centre and that of Google. It is a product derived from Landsat satellite imagery, entailing the processing of nearly 4 million Landsat images acquired over 34 years (16/03/1984-31/12/2018) in which water surfaces were monitored with their dynamics and occurrence being mapped over time [33]. Hence, it is highly pertinent to use this database at a 95% threshold, and hence nearly permanent water, to obtain water classification samples and derive signatures from optical imagery for a sample based classification.

### 5.2.2 **VHR optical sensors and Sentinel-2**

Pléiades-HR, SPOT 6/7 and Worldview-2/3 sensors are the most common VHR datasets used in rapid mapping of disaster events context. Pléiades-HR system has a high revisit capacity thanks to its twin satellites, whereas Digital Globe has this and WorldView-3 which has a middle infra-red spectral band, highly useful in water detection.

Pléiades-HR is an optical observation system with a constellation of two satellites. It was designed to offer a high acquisition capability with a revisit lower than 24 hours for both civilian and military needs. The Pléiades system was designed under the French-Italian ORFEO program. As prime contractor for the Pléiades system, the CNES (French Space Agency) contracted with Airbus Defence & Space (former EADS Astrium Satellites) to build the satellites and with Thales Alenia Space for the optical instrument. Spot Image is the official and exclusive worldwide distributor of Pléiades products and services under a delegated public service agreement. Pléiades-HR 1A was launched in December 2011 and Pléiades-HR 1B in December 2012. The system acquired data with 4 spectral bands (blue, green, red and near infrared) with a resolution of 2.8 m in vertical viewing, and with a resolution of 0.7 m in panchromatic mode. Moreover, the great agility of the satellites allows the acquisition of stereoscopic couples (or even triplet). Pléiades-HR also share the same orbital plane as the SPOT 6 and 7, forming a larger constellation with 4 satellites, 90° apart one from the other.

WorldView-3 is a commercial Earth Observation satellite owned by the U.S. company Digital Globe launched on 13 August 2014. WorldView-3 provides 31 cm panchromatic resolution, 1.24 m multispectral resolution (8-bands), 3.7 m SWIR (Short-Wave Infrared) resolution, and 30 m CAVIS (Clouds, Aerosols, Vapors, Ice, and Snow) resolution. The satellite has an average revisit time of less than 1 day and is capable of collecting up to 680 000 km² per day.

SPOT-6/7 are two identical satellites owned by Airbus DS (SPOT-6), a European company, and by Azerbaijan (SPOT-7), but operated by Airbus DS for rapid mapping purposes. The data from these satellites are of high relevance for rapid mapping purposes due to their very high precision (1.5 m) and their very large swath width (60 km). Within rapid mapping they are often used due to their availability to cover, often fires, and they are definitely an option for flood mapping.

Sentinel-2 is a European wide-swath, high-resolution, multi-spectral imaging mission. The full mission specification of the twin satellites flying in the same orbit but phased at 180°, is designed to give a high revisit frequency of 5 days at the Equator. The twin satellites of Sentinel-2 provide continuity of SPOT and Landsat-type image data, contribute to ongoing multispectral observations and benefit Copernicus services and applications such as land management, agriculture and forestry, disaster control, humanitarian relief operations, risk mapping and security concerns. Sentinel-2A (launched in 2015) and Sentinel-2B (launched in 2017) satellites are equipped with a single multi-spectral instrument (MSI) with 13 spectral bands in the visible / near infrared (VNIR) and short wave infrared spectral range (SWIR): four bands at 10 meters, six bands at 20 meters and three bands at 60 meters spatial resolution. The orbital swath width is 290 km. Moreover, Sentinel mission objective is to provide systematic acquisitions, with a free and open data policy.

VHR and Sentinel-2 data are complementary. Despite its “coarser” resolution, Sentinel-2 data are acquired automatically and do not require specific orders. They cover large areas and are free to access. These characteristics opened the way to several applications. Focusing over a chosen area, monitoring is easy to carry out (if the weather is clear of course). Advantage of VHR data is mostly their spatial resolution which allows bringing a detailed analysis, especially in landscapes where other sensors bring limited results (in urban areas for example). But VHR data access is not as easy as for Sentinel-2; acquisitions need to be ordered.

### 5.2.3 VHR optical and Sentinel-2-based flood processing chains

The development of an optical-based flood processing chain has been performed in two steps, leading to two dedicated tools having specificities linked to the input sensor:

- WATEX, a flood extraction tool dedicated to optical sensors (also functional with radar data);
- ExtractEO, an end-to-end flood processing chain dedicated to Sentinel-2, including the imagery download; this tool can be extended to other event types or thematic and other open source imagery (such as Sentinel-1).

#### 5.2.3.1 Optical data-based flood extraction tool

Based on the analyses performed within past projects, UNISTRA developed an optical data-based flood detection workflow and the associated tool, called WATEX, with a bonus to be also adapted to radar imagery. The aim was to have a simple, operational and fast procedure working in most cases (Figure 5-4).

The first step of the development was to work on the automatic generation of samples, and therefore signatures, using the Global Surface Water Occurrence product, and a 95% threshold. Standard optical satellite bands, or at least a selection of these, have been integrated as an input for signature generation and the classification. The tool is also able to ingest water indices as input for signature generation; however, the calculation of indices is not integrated in the tool and has to be performed apart. Initially, WATEX used the Maximum Likelihood classifier, but after several tests, other classifiers have been integrated such as SVM (Support Vector Machine) which seems to provide better results, and Random Forest.

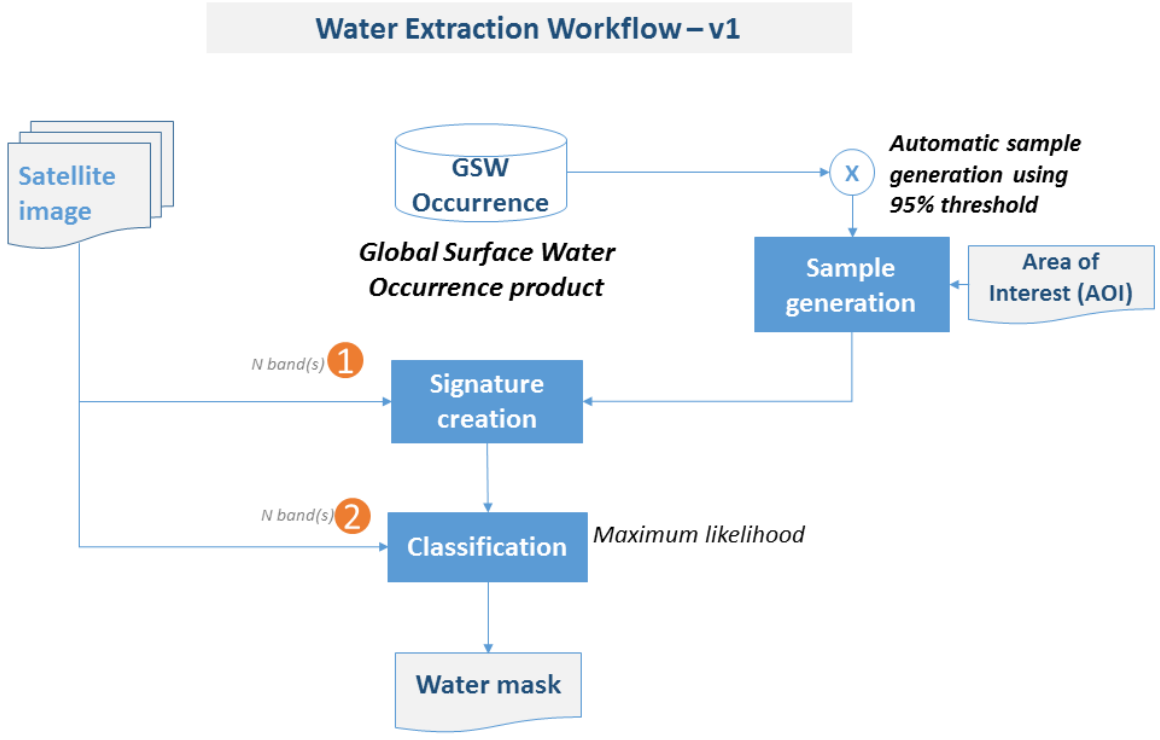


Figure 5-4: Optical data-based flood detection workflow

The automatic water extraction tool's interface is presented in Figure 5-5. As it is dedicated to both commercial and open satellite data, WATEX is not linked up to an automatic image search and download procedure, but the retrieval of satellite data is launched apart. It uses whatever satellite image you introduce to it. In fact, WATEX works indifferently whether the data are optical or radar. There are specific radar options, if needed, taking contextual pixel values into account. Its main characteristic is the automatic generation of water samples to

be used in the elaboration of water signatures which has been used to classify waterbodies. There are the following options:

- Possibility of GSW occurrence threshold adjustments;
- Possibility to include contextual radar threshold options
- Possibility to choose the algorithm (SVM or Random Forest).

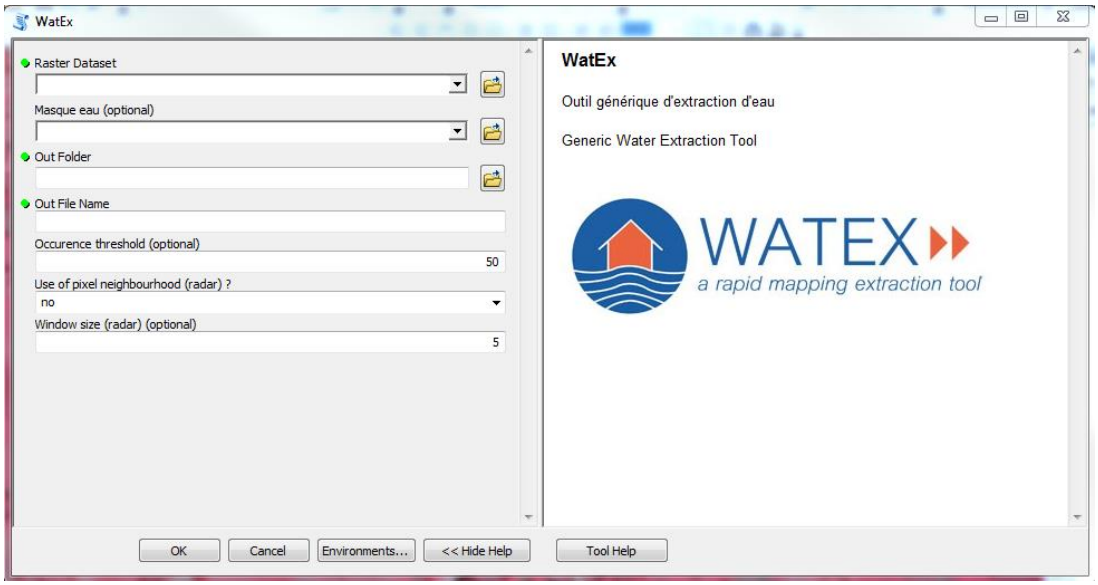


Figure 5-5: WATEX interface

In addition to WATEX, another tool, named WaToV (Water mask To Vector), has been developed to convert the raster water mask outputting from WATEX in vector Shapefile format (Figure 5-6). This tool integrates a Digital Elevation Model (DEM) – of user's choice – in order to generate slope information allowing to automatically or manually "clean" the result using slopes thresholds.

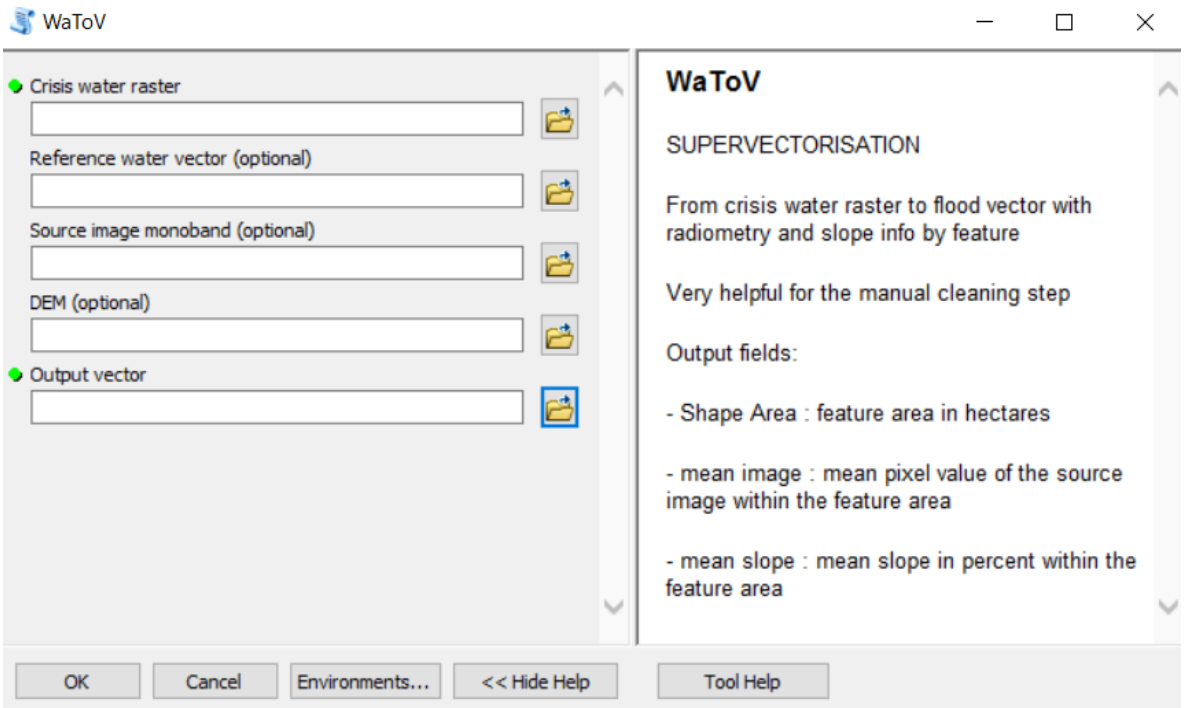


Figure 5-6: WaToV interface

### 5.2.3.2 Sentinel-2-based flood processing chain

For free and available satellite images such as Sentinel-2 data, UNISTRA worked on an end-to-end processing chain, from the data retrieval to the water detection, called ExtractEO.

The first step needs to involve an operator to specify at least an AoI and a date of interest, indicating to the processing chain which Sentinel-2 product(s) to download. All the products that fully or partially cover the AoI are then automatically downloaded.

The next step consists in the automatic processing of all Sentinel-2 downloaded products, as detailed below:

- Automatic water samples are extracted from the Global Surface Water database.
- Clouds are detected, following three different ways:
  - using the Sentinel-2 cloud mask, downloaded with the satellite image, but these can be very inaccurate,
  - using the well-known algorithm FMask, more accurate but very time-consuming,
  - using two threshold methods, one for L2A products (Braaten-Cohen-Yang cloud detector), one for L1C products (Hollstein cloud detector). These two methods are a good compromise between accuracy and time-consumption, especially for L1C methods, as the cirrus band is used to discard snow and clouds.
- An image stack is created from the Sentinel-2 bands and indices (usually, the stack is composed of the 3 RGB bands (B02, B03, B04) and 4 indices (MNDWI, AWEInsh, AWEIsh and Water Index).
- A model is trained thanks to the water samples and the image stack. Currently the model is a multi-layer perceptron (a good compromise between accuracy and computing time), but can be substituted by others, like SVM or random forest.
- The prediction is done on the whole image in case the flood happens also outside the AoI.
- A post-processing step in then enforced in order to:
  - sieve the image,
  - crop the prediction to the AOI,
  - merge the predictions if several Sentinel-2 products are composing the AoI,
  - eventually convert the prediction to a vector layer.

The workflow of this end-to-end processing chain is illustrated hereunder (Figure 5-7).

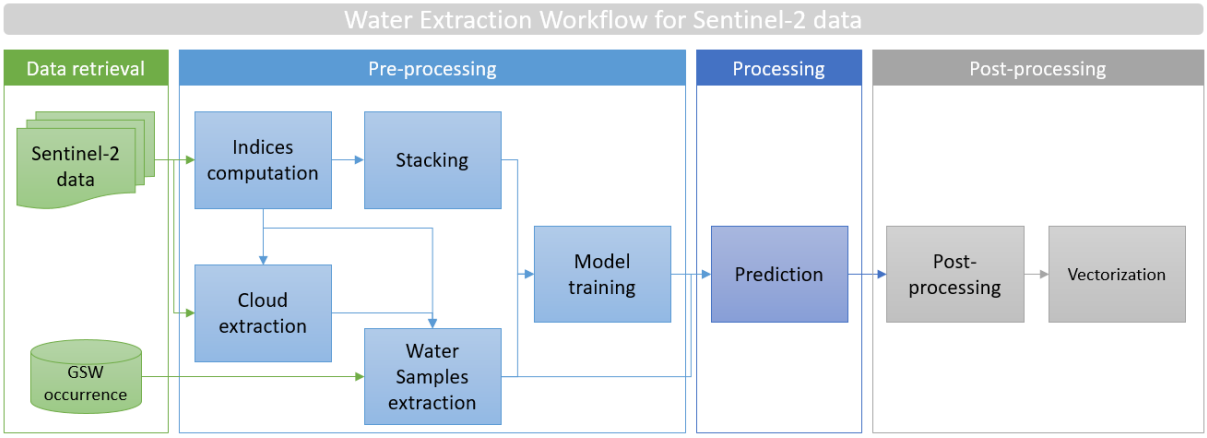


Figure 5-7: Current operational Sentinel-2 data-based flood detection workflow

The chain has been coded in Python and has to be seen as a plugin chain. Some can be added when developed (ie. Landsat management), and some can be discarded if useless (i.e. Cloud extraction for cloudless image).

Note that some work still needs to be done to improve the processing chain:

- A better post-processing involving Digital Elevation Models (DEMs) has to be done in order to ensure an optimal cleaning of the product,
- A more user-friendly Graphical User Interface needs to be set up,
- Some optimizations have to be done to ensure a better computing time.

### 5.2.4 **Products**

The products obtained with the VHR optical and Sentinel-2 flood processing chains are water masks which give an overview of the visible extent over an area affected by floods at a certain time.

The spatial resolution and coverage of flood masks depend on the specification of the data used. With Sentinel-2 acquisitions, the spatial resolution of flood mask is 10 m as VNIR bands of the product (Figure 5-8). With VHR data, flood masks will be more detailed (Figure 5-9).

The flood mask result is a binary GeoTIFF raster layer (0: no water; 1: water), also provided as vector format (ESRI Shapefile and GeoJSON), showing the water extent as a polygon.

The produced VHR and Sentinel-2 flood extent vector products are published as a WMS or WFS service containing flood polygons. The flood services contain all available detections for the areas of interest.

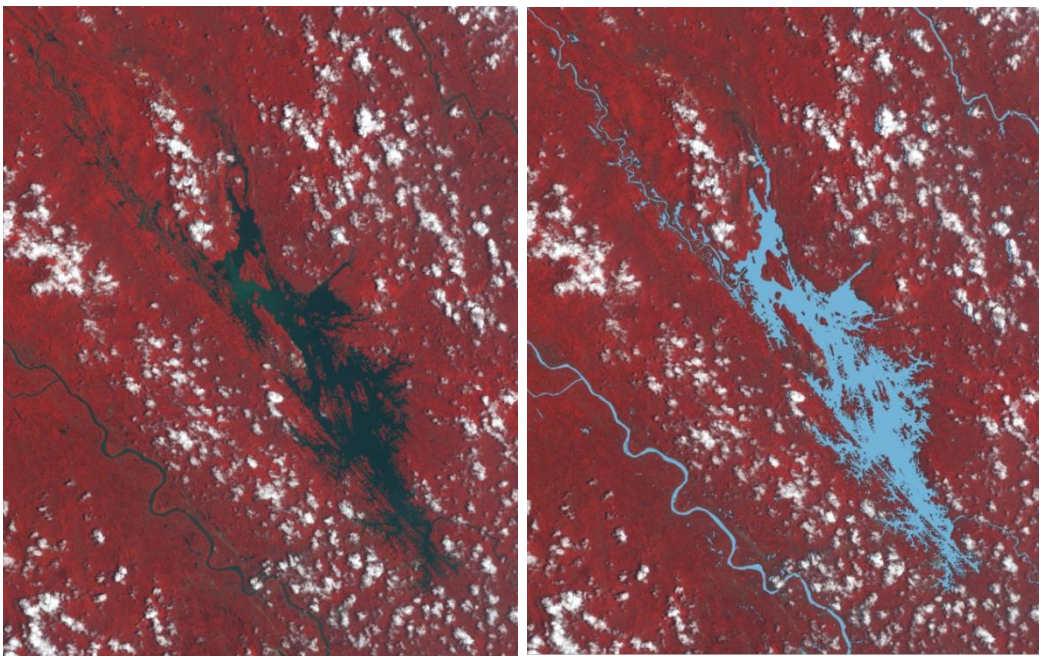

Figure 5-8: Sentinel-2 water extraction - Thác Bà Lake, Vietnam, August 2019.

Figure 5-9: Pléiades-HR water extraction - Forbes, Australia, September 2016.

## *5.3 Fire hot spot detection*

### 5.3.1 **MODIS-based fire hot spot processing chain**

The MODIS instrument is on board the Terra (EOS AM-1) and Aqua (EOS PM) satellite platforms as part of the NASA international Earth Observing System (EOS). Each MODIS sensor provides daily image coverage of almost the entire surface of the Earth in the mid to high latitudes, producing observations in 36 spectral bands at moderate spatial resolutions (250, 500, and 1000 m). Daily, the thermal information is collected with a spatial resolution of 1000 m, twice by each sensor, providing up to four thermal observations daily.

The MODIS images used for fire detection are acquired from two direct broadcast receiving stations from DLR located in Oberpfaffenhofen and Neustrelitz, Germany.

The detection of High Temperature Events (HTE) is performed using the MOD14 algorithm. MOD14 is well documented and tested in operational services and guarantees comparability and reproducibility as well as a standardized international acknowledged product. HTE detection is performed using a contextual algorithm that exploits the strong emission of mid-infrared radiation from wild land fires (land-use fires, wildfires burning in forests, savannahs, peat lands and other ecosystems) and other fires or heat sources (e.g., gas flares, volcanoes, industrial sites). The MODIS active fire algorithm can routinely detect fires of an average size of 900 $m^2$. Each pixel which is detected as fire pixel or ‘hot spot’ is

characterized by the fire radiative power (FRP). The FRP is the total rate of emission of radiative energy from the fire and is expected to depend on the rate of combustion of biomass in the fire. For the processing, the most current version of the NASA algorithm (v6.0) is used.

The output of the MODIS Fire Service is the location of hot spots in near-real time for Europe and surrounding countries, including, for every detected fire, information about:

- Latitude and longitude
- Administrative boundaries
- Vegetation and land cover (CLC2000, GLC2000)

### 5.3.2 **Products**

The detected pixel locations are transferred into a vector file containing the latitude and longitude information as well as fire radiative power and auxiliary information.

These locations are integrated into a WFS service, containing all detections for the areas of interest for the seven recent days. They are updated as soon as new data becomes available. In this case, also a notification is generated by the system to inform concerned parties about the updated status using a publish/subscribe mechanism. The WebHooks technology is utilized for implementing this functionality. This mechanism is used regarding all services published by DLR in the frame of HEIMDALL.

## *5.4 Burn scar mapping using Sentinel-2*

### 5.4.1 **Optical data-based burn scar detection**

In order to estimate the extent of the damage and to model the impact on the climate, as well as for planning in forestry and fire management, it is essential to have a precise knowledge regarding the location, the extent, and the frequency of fire incidents [34]. Therefore, the detection of burn scars is an important tool to monitor the total extent, as active fire-based approaches are only able to provide information about the current state of the fire event at the moment of the overflight [3].

In comparison to the spectral properties of the unburned areas before the fire event, burn scars are characterized by a rise in the visible and short-wave infrared radiation. In contrast, there is a loss in the near infrared wavelength range. This is due to the fact that the chlorophyll of healthy vegetation absorbs visible radiation and strongly reflects near infrared radiation. Short-wave infrared radiation shows a similar behaviour to radiation in the visible range, but the absorption is mainly caused by the liquid contained in the plants [35, 36].

Numerous methods have already been developed for the detection of burn scars. A distinction can be made regarding their different approaches in the procedures, the different classification methods and the different features used in the classification process.

In generally there are two approaches in the procedures: some of the algorithms are based on one phase, others are using two phases in the classification process, where the first phase is used to generate seed pixels that are most likely to be burnt. In the second phase, a refinement of the burned areas is done by investigating the neighbourhood of the seed pixels.

The methods can also be subdivided according to the classification methods used. Often, the detection of burnt areas is carried out using threshold-based criteria. A distinction can be made between procedures with fixed and dynamic threshold values. Other methods are using logistic regression analyses to generate a model for the identification of burn scars or spectral unmixing. Furthermore, there are approaches with Maximum Likelihood or Minimum Distance to Means Methods. Other approaches are using machine learning, e. g. neural networks or SVMs. In contrast to most pixel-based methods, there are also some object-based classification methods which first perform a segmentation creating objects and then

examining the properties of these objects in the subsequent classification instead of the properties of the individual pixels.

Furthermore, one can distinguish between different burn scar detection approaches regarding the information they use in the classification process. In general there are three types used: spectral, temporal and contextual information. The observed reflectances as well as various spectral indices are used as spectral information. Some approaches are using mono-temporal information whereas others are based on multi-temporal information. Most approaches use bi-temporal information in the form of spectral differences between the pre- and post-disaster images. Others use time series information for the identification of the burned areas. In addition to that, there are approaches using contextual information, such as the neighbourhood, this especially includes the two-phase methods.

### 5.4.2 **Methodology for Sentinel-2-based burned area detection**

For the provision of burn scar masks within HEIMDALL a fully automatic burn scar processor based on Sentinel-2 data is developed to enable systematic monitoring. For the characteristics of the Sentinel-2 sensor see Chapter 5.2.2.

The fully automated processing chain includes the download and pre-processing of the Sentinel-2 data, as well as an unsupervised classification. The Sentinel-2 data are automatically downloaded through a Python-based script, which routinely queries the ESA Sentinel Data Hub for new acquisitions over the area of interest and downloads them. Subsequently, an atmospheric correction is performed with the S-2 Level-2A Prototype Processor (Sen2cor) from the freely available ESA Sentinel-2 Toolbox. The classification is a two-phase algorithm, where the first phase serves to identify seed pixels which have a high probability to be related to burnt areas. In the second phase, a refinement of the burned areas is accomplished by examining the neighbourhood of the seed pixels.

The final burn scar masks are stored in raster and vector format, respectively**.**

### 5.4.3 **Products**

The products derived by the Sentinel-2 burned area processing chain is the burned area masks which give an overview of the extent of recent burn scars at a certain time with respect to the pre-disaster situation.

The spatial resolution of the Sentinel-2 burn scar masks is ~10 m corresponding to the highest resolution of the three Sentinel-2 resolution types (10/20/60m see Chapter 5.2.2). Binary burn scar masks are provided within HEIMDALL in both raster (GeoTIFF) and vector (ESRI Shapefile) format to the end users.

These locations are integrated into a WFS service. They are updated as soon as new data becomes available. In this case, also a notification is generated by the system to inform concerned parties about the updated status using a publish/subscribe mechanism. The WebHooks technology is utilized for implementing this functionality.

## *5.5 Fire Severity*

### 5.5.1 **Optical data-based fire severity**

In order to complement the burn scar mapping, UNISTRA developed fire severity processing chains providing the level of fire severity within the burnt areas, which is a useful input for damage assessment.

Two different approaches to map fire severity have to be distinguished, depending on the characteristics of the images being used:

- Images with Short Wave Infrared (SWIR) channel (Sentinel-2, Landsat-8, WorldView-4 in some cases)
- Images without SWIR channel (SPOT 6/7, Pléiades-HR, WorldView-2/3/4 in most cases).

The method with SWIR channels is simple and widely used, especially by the US Fire Science community (USFS). The method uses the dNBR (explained below) to indicate the ecological impact of a fire on a landscape. Low and high severity does not mean a higher or lower level of fire but indicates what has been lost in terms of vegetation due to the fire. This is the ecological severity.

The method without SWIR is a stop gap that indicates whether or not vegetation is present within the fire affected areas before and after a fire and within the burn scar. Unfortunately, the vast majority of agile, rapidly available satellite images do not have a SWIR channel.

Testing on multiple fire cases and landscapes have been performed and revealed the efficiency of these processing chains, which are now also used within Copernicus EMS Rapid Mapping and shared with the International Working Group on Satellite-based Emergency Mapping (IWG-SEM) as standard guidelines.

### 5.5.2 **Fire severity: Methodology with** SWIR channels

In addition to giving the fire severity, the result of the methodology described below can help the operator to digitize and/or validate the burn scar area.

The prerequisite is to use pre- and post-fire images acquired as close as possible to the fire event.

The first step is to calculate the Normalised Burn Ratio (NBR) [37] index for pre and post-fire images (Figure 5-10):

$$NBR = (NIR – SWIR) / (NIR + SWIR)$$

Then the difference dNBR can be calculated as follow (Figure 5-10: Optimal pre and post Sentinel-2 band combinations, resulting pre and post NBR's and resulting dNBR):

$$dNBR = NBR_{pre\text{-}fire} - NBR_{post\text{-}fire}$$

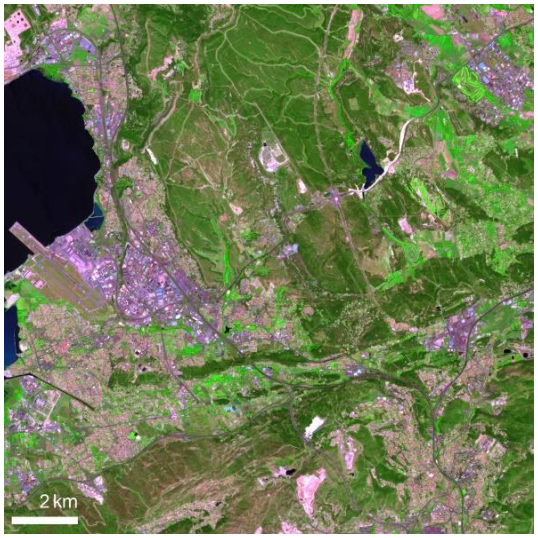

Pre-event Sentinel-2

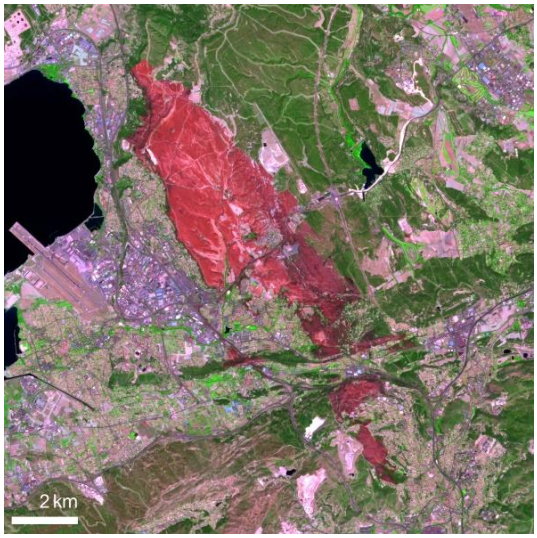

Post-event Sentinel-2

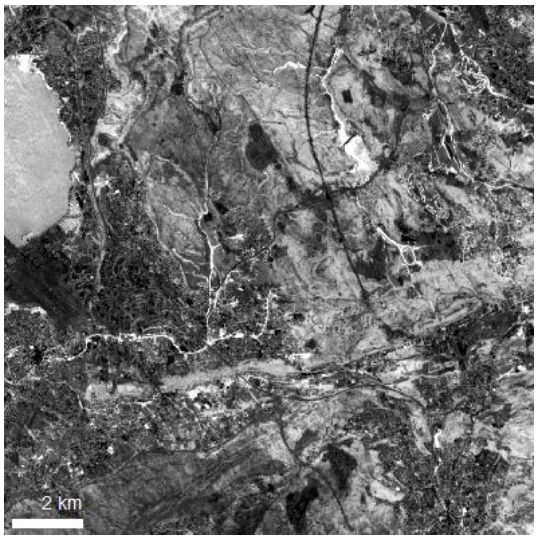


Pre-event Sentinel-2-NBR

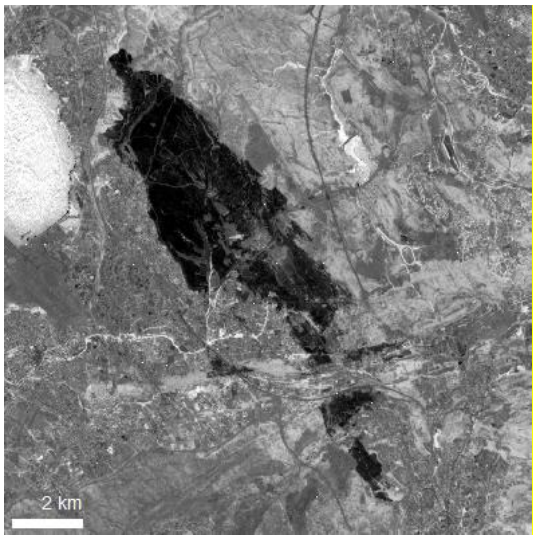


Post-event Sentinel-2-NBR

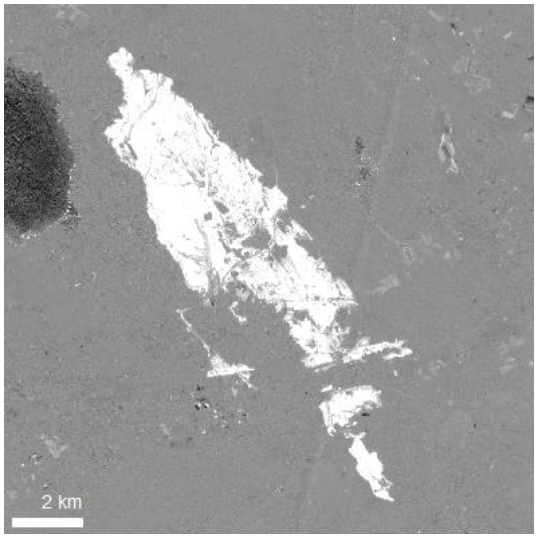


dNBR derived from pre and post-event Sentinel-2 images

Figure 5-10: Optimal pre and post Sentinel-2 band combinations, resulting pre and post NBR's and resulting dNBR - Rognac fire event, France, August 2016.

The next step consists of classifying the result with the predetermined classes by US Forest Service (Table 5-13 and Figure 5-11).

Table 5-13: US Forest Service dNBR fire severity classification

| **dNBR** | **Fire severity** | |
|---|---|---|
| <= 0.1 | Unburned | |
| 0.1 to 0.27 | Severity low | |
| 0.27 to 0.44 | Severity low to moderate | |
| 0.44 to 0.66 | Severity moderate to high | |
| > 0.66 | High severity | |

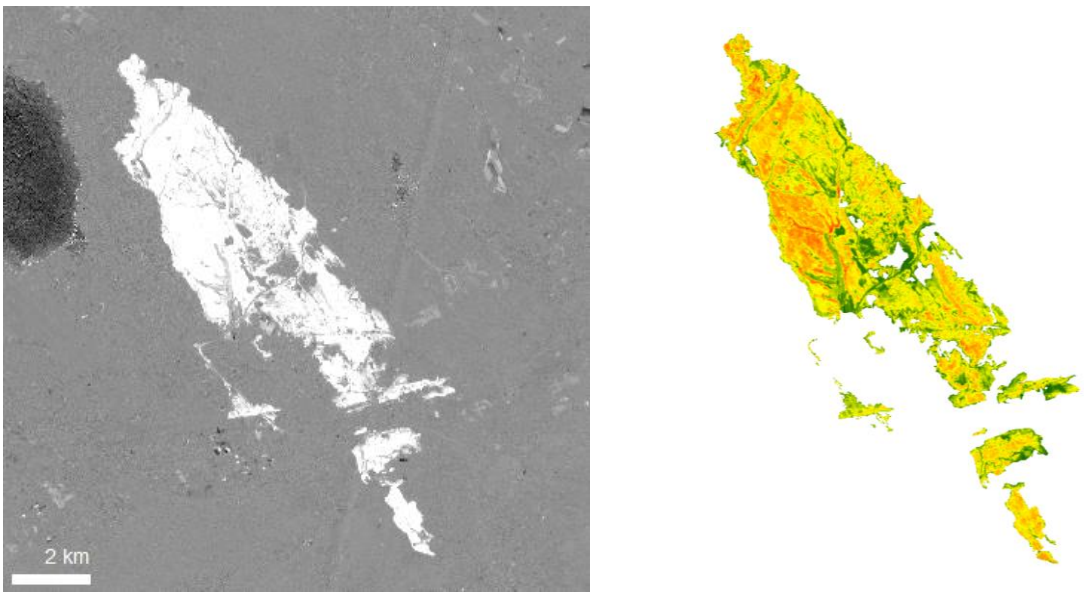


dNBR before classification dNBR after classification

Figure 5-11: Deriving a dNBR based fire severity index

The last step of the fire severity assessment is to clip the severity result by the fire extent extracted beforehand. Either the images are pre-clipped or clipped after dNBR calculation (Figure 5-11).

A simplified fire severity classification can be proposed in order to improve the readability of the fire severity result. The “Unburned” class is removed whereas the “Severity low to moderate” and “Severity moderate to high” classes are grouped into one class (Table 5-14).

Table 5-14*:* Comparison between dNBR classes and simplified severity classes

| **dNBR** | **Fire severity classes** | | **Simplified classes** | |
|---|---|---|---|---|
| <= 0.1 | Unburned | | Unburned | |
| 0.1 to 0.27 | Severity low | | Low severity | |
| 0.27 to 0.44 | Severity low to moderate | | Moderate severity | |
| 0.44 to 0.66 | Severity moderate to high | | | |
| > 0.66 | High severity | | Moderate severity | |

## 5.5.3 **Fire severity: Methodology without SWIR channels**

This section presents different methods to assessing fire severity using images not containing a Short Wave Infrared (SWIR) band.

The testing of NDVI’s and difference NDVI’s (dNDVI) of pre and post-event SPOT-6/7 data are analysed in order to define the most pertinent methodology. The testing is made exclusively in the burn scar areas.

Furthermore, pre and post-event Sentinel-2 imagery is used to complement the fire severity analysis, enabling a comparison with and without SWIR data. The operator validated fire severity results derived from the Sentinel-2 data are considered to be the layer of reference.

The results of the SPOT-6/7 and Sentinel-2 image processing and classification, displayed in Figure 5-12, indicate that the simple use of the post fire NDVI has the worst results with large shadowed areas being classified as badly affected. Otherwise, the dNDVI results look

promising when compared to the dNBR results. Moreover, the dNDVI seems to be a good alternative helping to detect if vegetation is still photosynthetic in shadowy areas.

Furthermore, the correlation of the dNDVI and the dNBR has been noted through scatterplots that show that they are someway related. Hence, dNDVI is a good way of calculating fire severity and could be used in a fire severity classification procedure when no SWIR is available.

| **Methodology** | **Results** | |
|---|---|---|
| Classification based on post event VHR image using supervised classification | | 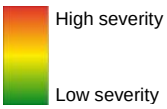  |
| Classification based on pre and post-event Sentinel-2 NBR data (dNBR) | | 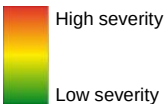  |
| Classification based on SPOT-6/7 NDVIs differences<br>(NDVI pre - NDVI post) | 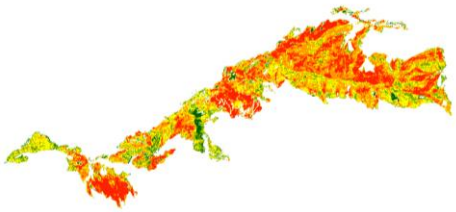 | 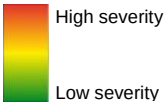  |
| Classification based on Sentinel-2 NDVIs differences<br>(NDVI pre - NDVI post) | | 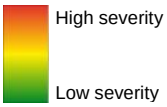  |

Figure 5-12: Results of different fire severity methodologies

Furthermore, comparison of dNDVI values obtained from Sentinel-2 and SPOT-6 dNDVI in the burn scar shows a high similarity which can be used in combination (Figure 5-13). The three classes correspond to dNBR derived nomenclatures and their dNDVI correspondences are described in Table 5-15. The dNBR classes are used to obtain dNDVI signatures and classes.

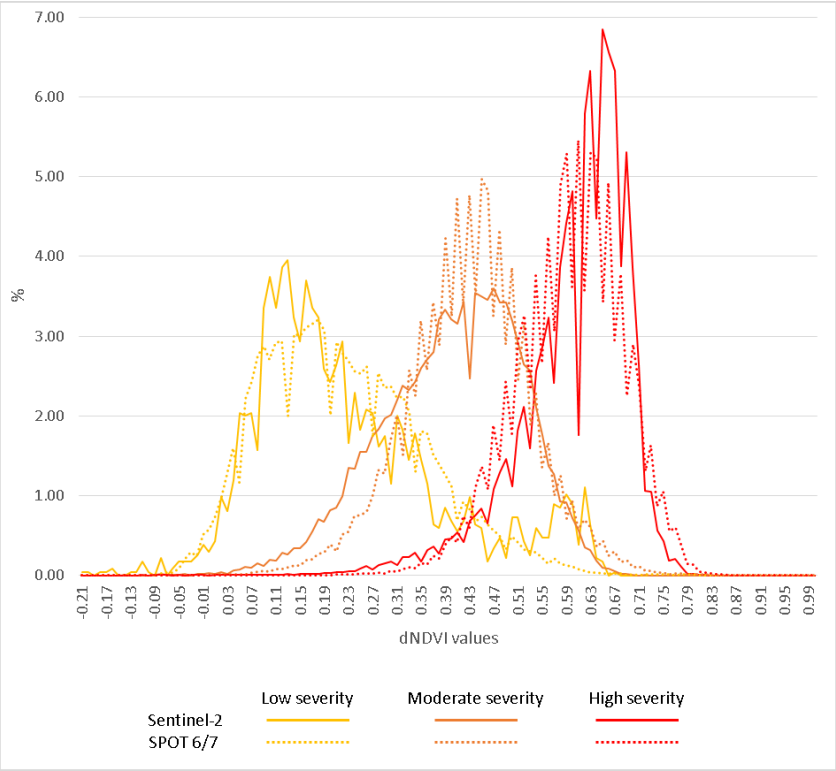


Figure 5-13: Results of fire severity dNDVI methodology. The two middle classes are regrouped afterwards.

Table 5-15: Fire severity class description and corresponding dNDVI values which work for Sentinel-2 and SPOT-6/7 dNDVI calculation.

| dNDVI per fire severity class | Class description | Colour |
|---|---|---|
| dNDVI <= 0.3 | Low severity | |
| 0.3 > dNDVI <=0.55 | Moderate severity | |
| dNDVI >0.55 | High severity | |

## 5.5.4 **Fire Severity Products**

The product obtained in output of the fire severity processing chains is a classification giving the fire severity in the burnt area.

The spatial resolution of the fire severity depends on the data used as input. With Sentinel-2 data, the spatial resolution of the fire severity is 10 m (SWIR channel interpolated at 10 m). With VHR data, the fire severity will be more detailed.

The fire severity result (Figure 5-14) is a classified raster GeoTIFF layer (0: High severity / Destroyed; 1: Moderate severity / Damaged; 2: Low severity / Possibly damaged) which is also provided as vector format (ESRI Shapefile and GeoJSON).

The fire severity products are published as a WMS or WFS service containing fire severity polygons on the HEIMDALL Service Platform.

Figure 5-14: Fire severity product based on Pléiades-HR data - La Jonquera fire event, 24/07/2012

## *5.6SAR-based landslide monitoring*

### 5.6.1 **Detection of landslides using SAR data**

The application of interferometric techniques to SAR data to detect and monitor landslides dynamic is an established process, and the achievement of the extent and the spatio-temporal evolution of instable slopes has been demonstrated in several papers and projects. Particular examples of studies related to geohazard and subsidence can be found in [38-40]. Several methodologies and processing tools have been developed (see [41-44]). Mainly based on the implementation of the Persistent Scatterer Interferometry (PSI) technique [45] or similar approaches; a review of all the PSI implementations is available for example in [46] and [47]. Although, some aspects of the technique are not straightforward, such as the geometric limitation of SAR acquisition, the capability of measuring deformation only in the line of sight of the satellite, and the spatio-temporal noise, an operational tool is now readily available to the user. In addition the characteristics of the Sentinel-1 constellation allow accomplishing long term monitoring planning, at a regional scale, in any location globally.

### 5.6.2 **Sentinel-1-based landslide monitoring chain**

In Figure 5-15 the flowchart of the methodology developed and applied by CTTC to use Sentinel-1 SAR images for the landslide detection and monitoring is provided.

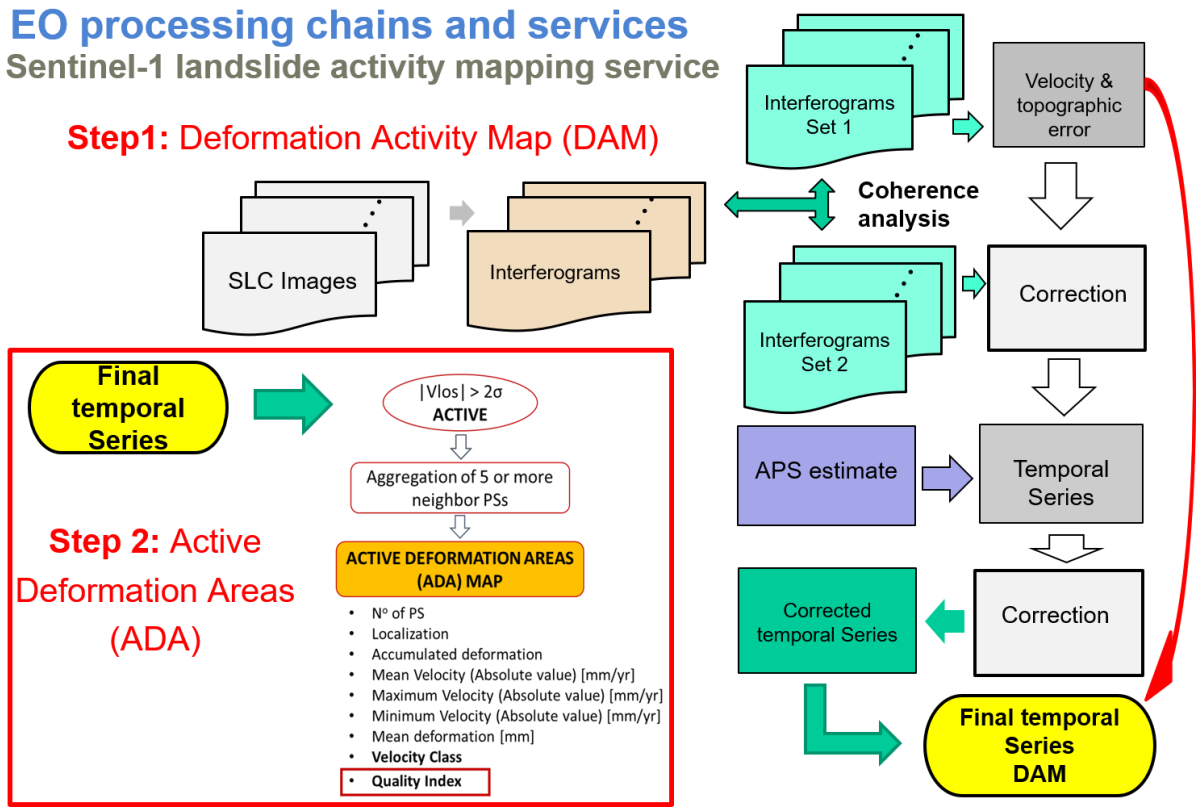


Figure 5-15: Workflow of the developed methodology to produce DAM and ADA

The developed methodology can be summarized in three main blocks:

I. The Processing block which consists of the processing of Sentinel-1 data in order to obtain the preliminary deformation map.
II. Post-processing block which consists of the simplification of the preliminary deformation map, in order to improve both the reliability and the readability. The outputs of this block are the final Deformation Activity Map (DAM) and the *Active Deformation Areas* (ADA) map.
III. Geohazard management block which consists of the use of the ADA map along with other relevant information in order to update the existing knowledge and derive useful maps for the geohazard management activities. The main output of this block is the Geohazard Activity Map (GAM) and the Vulnerable Element Activity Map (VEAM) [48].

### 5.6.3 **Products**

Deformation maps and temporal series of selected area/pixels are provided as first product. The basic spatial resolution of the Sentinel-1 products is ~20m as provided by the Interferometric Wide swath (IW) mode.

The approach described in 5.6.2 also makes available, as a additional product, a map where novel or active deformation areas are identified, as potential landslides. In order to periodically assess their activity state and update the existing Landslide Inventory Map, the output from the post processing activities are compared to the existing data inventory.

The produced maps and database will be available in a specific web portal managed by CTTC, and accessible to the HEIMDALL concerned partners, through WMS or WFS standard, to integrate the products in the HEIMDALL platform.

## *5.7 Landslide mapping using Sentinel-2*

### 5.7.1 **Detection of landslides using optical data**

Landslides, as the name suggests, being large displacements of material, the use of optical data for their detection is relevant. Starting with high-resolution sensors (Landsat, SPOT1-4), studies are now performed using satellites with higher spatial, spectral, and temporal resolutions [34][34]. The development has been such that satellite and aerial images are now giving similar results for landslide inventories [35]. Furthermore, a cost-benefit analysis suggests that stereo satellite photo-interpretation is usually more effective than stereo airborne photo-interpretation for landslide hazard assessment over large areas [36].

A first method to exploit data would be photo-interpretation. By looking at a post-event image and comparing it with a pre-event one, the user can detect landslides. While this method is consistent for shallow, well distinguishable landslides, problems arise when trying to detect deep-seated ones. Indeed, deep landslides are characterised by a slow moving speed and are not visible between two temporally close images, like a shallow landslide would be. The boundary between the stable ground and the falling mass is more transitional and different factors make it hard to detect, such as colonising vegetation or earth filling [49]. Photo-interpretation is time consuming, requires VHR images and a trained eye for a good landslide mapping and is subject to human error.

Keeping in mind the increasing volume of data to be analysed, methods are developed to automatically extract landslides envelops. A first category of algorithms consists of pixel-based classifications. These methods consider the spectral information of each pixel independently of its neighbours. As stated by [50], considering the resolution of EO data and the typical size and distribution of landslides, pixel-based methods may be prone to error. Adding the spatial context using an object-based approach allows considering geometric features such as shape properties or per-object averaged spectral or geomorphologic properties [51]. The size of aggregations can be different, even variable within the same method as proposed in [52]. In [53] a region-based active learning algorithm, which belongs to supervised classification techniques, was performed on multi-temporal very high-resolution optical images to recognize large-scale shallow landslides. Automated processing and the visual analysis of RapidEye data, combined with field reconnaissance and historical records, have been exploited to detect and characterise 250 landslides in Southern Kyrgyzstan [54].

### 5.7.2 **Sentinel-2 landslide detection chain**

#### 5.7.2.1 Simple multi-thresholding

A pixel-based approach has been chosen, even though it is generally less accurate than an object based chain, as it allows an automatic process and more importantly, it is considerably faster. The methodology relies on a basic principle which is the sudden disappearance of vegetation where a landslide has occurred. Change detection between reference and crisis images highlights this disappearance in vegetation. A threshold is applied on the result on NDVI (Normalized Difference Vegetation Index) difference computation. As the index used is normalised in theory the threshold should not have to change with a different set of data, on condition that there is vegetation in the reference image. This is important because the methodology has been built regarding the reproducibility of the process. An additional process allows the reduction of false alarms by thresholding slopes using a DEM. Landslides occur on steep slopes; detected objects on flat terrain can be removed. False detection provoked by clouds can be removed using the band 10 from Sentinel-2 datasets (Figure 5-16). The workflow is called SlidEx.

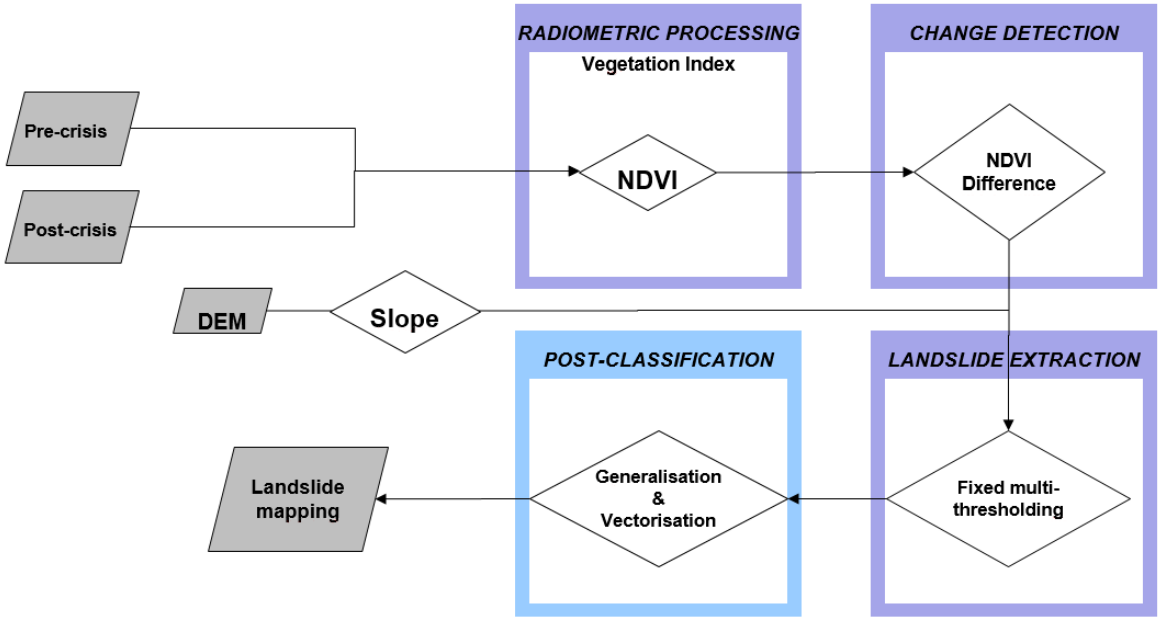


Figure 5-16: SlidEx automatic landslide detection workflow for Landsat-8/Sentinel-2 data

Figure 5-17 shows the input parameters required for it to function. The algorithm is based on change detection. Therefore, a pre-event and a post-event image is necessary. Like the water extraction tool, its use can be generic. Sentinel-2 is not compulsory for the tool to work, it just requires Red and NIR bands. Changes will be done to allow the user to select the bands, making the tool more flexible and transparent. The output is a single binary raster showing extracted landslides.

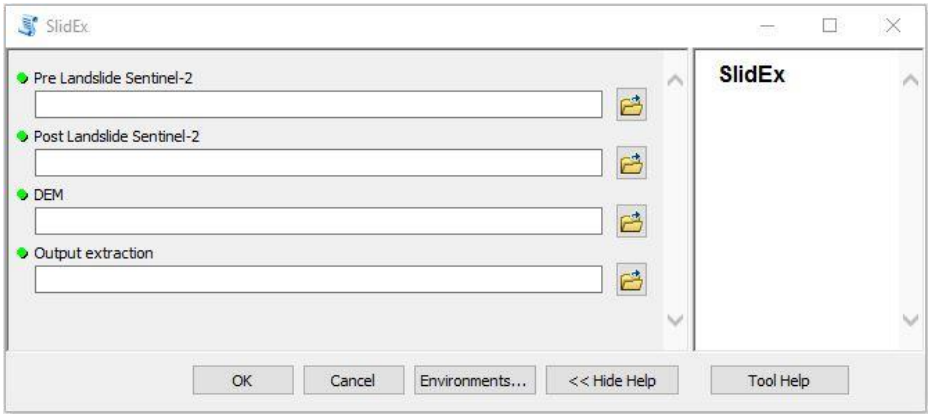


Figure 5-17: SlidEx interface

### 5.7.2.2 Supervised classification of Sentinel-2 data

A second more robust methodology has been applied for Sentinel-2 data, based on the architecture presented in 5.2.3.2. The aim is to tackle problems from the previous version such as false positives induced by clouds, by using more information than the NDVI.

The process consists in the automatic processing of any Sentinel-2 downloaded products, as detailed below:

- Training samples are generated by the operator in ESRI shapefile format. Two classes at least must be present: “landslide” and any other class.
- A DEM covering the AOI is imported, often SRTM or EU-DEM

- An image stack is created from the Sentinel-2 bands, the DEM and indices (usually, the stack is composed of the 3 RGB bands (B02, B03, B04) and any vegetation indices (NDVI, EVI etc.).
- A model is trained thanks to the training samples and the image stack. Currently the model is a random forest.
- The prediction is done on the whole image.
- A post-processing step in then enforced in order to:
    - sieve the image,
    - crop the prediction to the AOI,
    - merge the predictions if several Sentinel-2 products make up the AoI,
    - eventually, the prediction is converted to a vector layer.

Note that some work still needs to be done to improve the processing chain:

- A more user-friendly Graphical User Interface needs to be set up,
- Some optimizations have to be done to improve computing time.

### 5.7.3 **Products**

The products obtained with the Sentinel-2 landslide processing chain are masks which give an overview of the visible landslide extent over an area affected at a certain time. The spatial resolution of the masks is 10m, the same as for Sentinel-2 VNIR bands. The mask extent is the same as the intersection of the pre and post image extents. The output format is a binary raster or vector (ESRI Shapefile), showing the landslide's extent.

The next series of figures (Figure 5-17 - Figure 5-26) show the results after applying the defined workflow. Three cases are presented: the Sichuan landslide (24th of June 2017 in Xinmo village, China), the Freetown landslide (14th of August 2017 in Freetown, Sierra Leone) and the Kumamoto landslides (16th of April 2016 in Kumamoto, Japan).

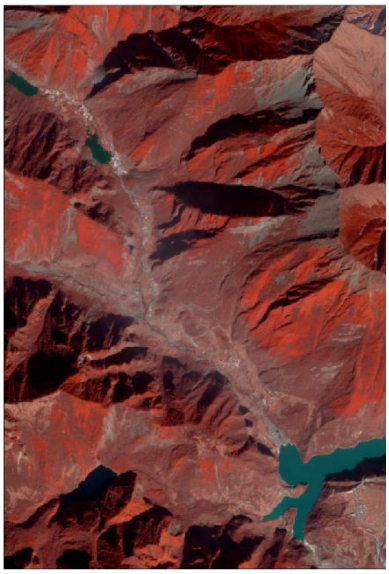

Figure 5-18: S2 reference image (Sichuan, 19/02/2017)

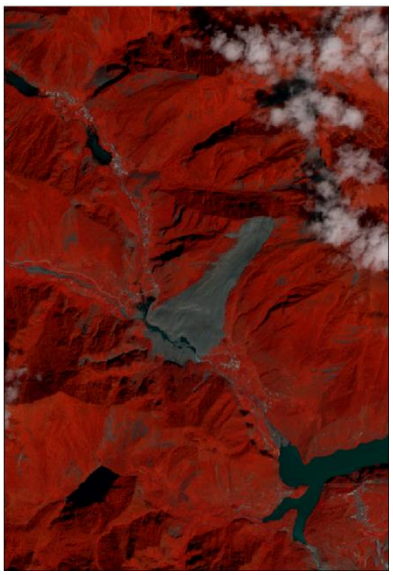

Figure 5-19: S2 crisis image (Sichuan, 07/09/2017)

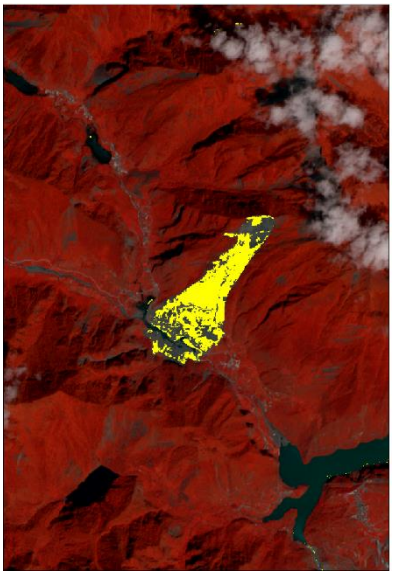

Figure 5-20: Landslide detection by double threshold on pre/post disaster NDVI difference and slope

Figure 5-21: S2 reference image (Freetown, 01/02/2017)

Figure 5-22: S2 crisis image (Freetown, 08/11/2017)

Figure 5-23: Landslide detection by double threshold on pre/post disaster NDVI difference and slope

Figure 5-24: S2 reference image (Kumamoto 03/03/2016)

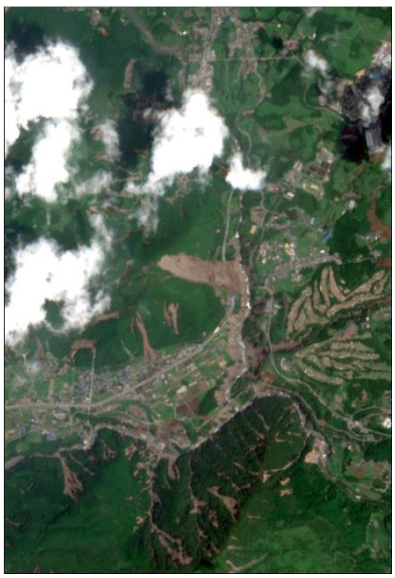

Figure 5-25: S2 crisis image (Kumamoto 10/08/2016)

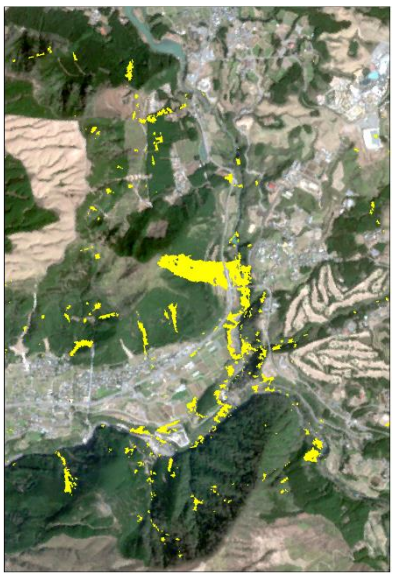

Figure 5-26: Landslide detection by double threshold on pre/post disaster NDVI difference and slope

The tool has been used during the CNES Charter call over Japan during the torrential rainfall of early July 2018. A large number of landslides occurred in the area of Kure, Japan. By using the landslide extraction tool, time was saved for crisis information extraction. Operator intervention was required for adjusting the threshold in NDVI difference and for cleaning the layer. Making the NDVI difference threshold dynamic, either as an input of the tool by the user, or automated calculation could be an improvement of the actual tool.

This example also illustrates the tool capacity to use different data. The pre event image (Figure 5-27) was Sentinel-2 data but the post event image used was Pléiades 1A data (Figure 5-28, Figure 5-29).

Figure 5-27: S2 reference image (16/06/2018).

Figure 5-28: Pléiades 1A crisis data (09/07/2018)

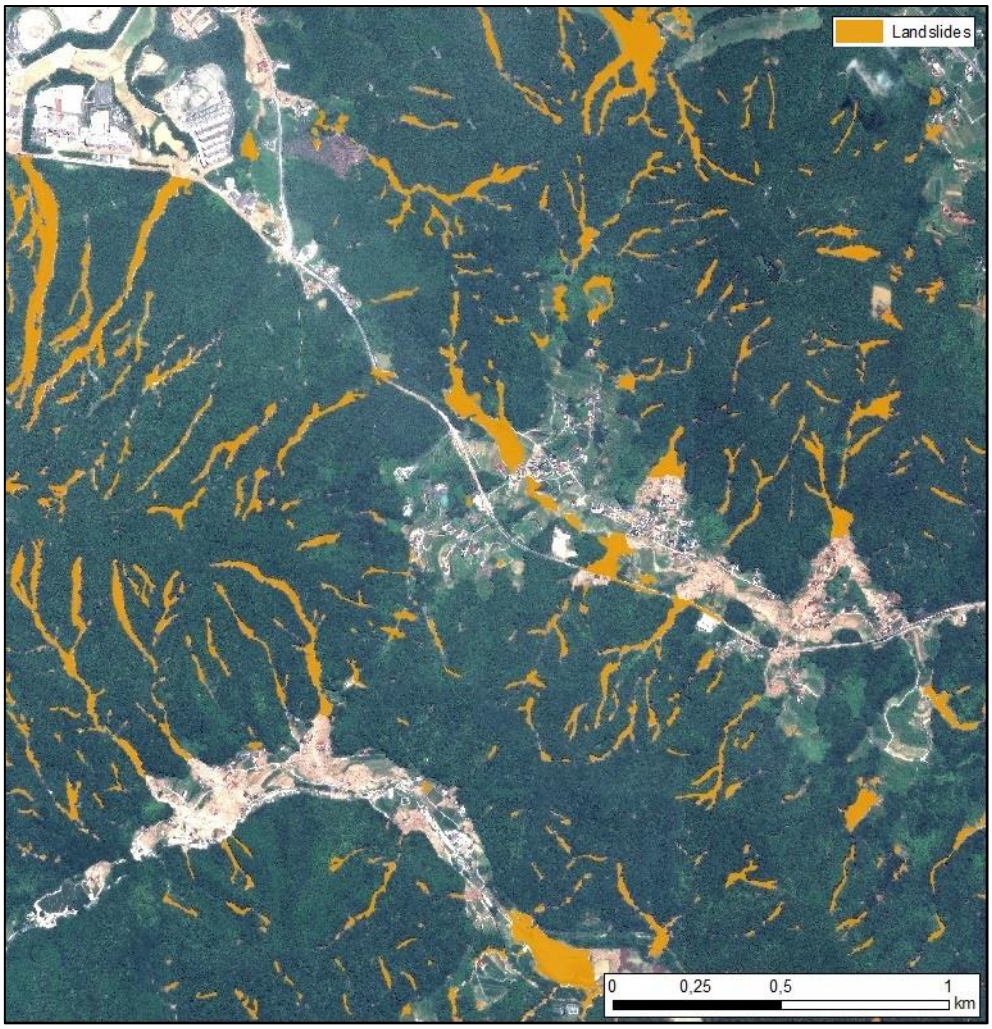


Figure 5-29: Landslide extraction over Kure during early July 2018 rainfall (Pléiades 1-A, © CNES, distribution Airbus Defence and Space)

The Sentinel-2 landslide extent vector products (Shapefile and GeoJSON formats) are published as a WMS within HEIMDALL. The landslide services contain all available detections for the areas of interest.

# 6 Test Plan

For technical requirements defined in Section 2 the following tests were performed:

Table 6-1*:* TS_EO_01.

| **Test ID** | *TS_EO_01* |
|---|---|
| **Requirements to be verified** | • TR_DataEO_1 |
| **Test objective** | To verify that the user is able to visualize the burnt scars and active fire hot spots in the HEIMDALL GUI. |
| **Test procedure** | 1. The user selects burn scars and active fire hot spots for an area of interest. |
| **Test prerequisites/ configuration** | • GUI connected to the HEIMDALL system |
| **Success criteria** | Correct visualization of burn scars and active fire hot spots for an area of interest. |
| **Results analysis** | *The test has been performed in a lab environment.* |
| **Success** | Passed |

Table 6-2*:* TS_EO_02.

| **Test ID** | *TS_EO_02* |
|---|---|
| **Requirements to be verified** | • TR_DataEO_2 |
| **Test objective** | To verify that the user is able to visualize the flood extent layers provided by project partners' automatic flood extraction systems in the HEIMDALL GUI. |
| **Test procedure** | 1. The user selects flood layers for an area of interest. |
| **Test prerequisites/ configuration** | • GUI connected to the HEIMDALL system |
| **Success criteria** | Correct visualization of flood layers for an area of interest. |
| **Results analysis** | *The test has been performed in a lab environment.* |
| **Success** | Passed |

Table 6-3*:* TS_EO_03.

| **Test ID** | *TS_EO_03* |
|---|---|
| **Requirements to be verified** | • TR_DataEO_4 |
| **Test objective** | To verify that the user is able to visualize information on the landslide extent based on Sentinel-2 data in vector and raster format as well as information about the movement of landslides based on Sentinel-1 data in the HEIMDALL GUI. |
| **Test procedure** | 1. The user selects landslide layers based on Sentinel-1 and Sentinel-2 data to |

| | |
|---|---|
| | visualize the extent and/or movement of the landslide. |
| **Test prerequisites/ configuration** | • GUI connected to the HEIMDALL system |
| **Success criteria** | Correct visualization of landslide layers based on Sentinel-1 or Sentinel-2 data for an area of interest.<br>Correct visualization of information related to the landslides. |
| **Results analysis** | *The test has been performed in a lab environment.* |
| **Success** | Passed |

# 7 Conclusions

This document presents specifications of the Earth Observation processing chains and derived products provided to the HEIMDALL Service Platform. The products provide disaster-related information in the context of fires, floods, and landslides to support decision makers and incident commanders during crisis situations, for preparation and in the aftermath. These products are automatically and semi-automatically derived based on various optical and radar Earth Observation data sets by the following processing chains:

- Automatic Sentinel-1 and TerraSAR-X flood processing chains
- Automatic Sentinel-2 burn scar mapping chain
- Automatic MODIS-based hotspot service for wildfire detection
- Automatic Sentinel-2 flood processing chain
- VHR optical flood processing chain
- Sentinel-2 landslide mapping chain
- Processing chain for updating landslide activity based on Sentinel-1 interferometric data
- Processing chain for fire severity estimation

Different EO-based products, which are derived from the implemented processing chains in the frame of floods, landslides and fire events and which have been integrated into the HEIMDALL Service Platform for demonstration purposes are visualized and described in D5.3 *EO Tools and Products.*

# 8 References

[1] Twele, A., Cao, W., Plank, S. & Martinis, S., 2016. Sentinel-1-based flood mapping. A fully automated processing chain. International Journal of Remote Sensing 37 (13). 2990–3004.

[2] Martinis, S., Kersten, J. & Twele, A., 2015. A fully automated TerraSAR-X based flood service. ISPRS Journal of Photogrammetry and Remote Sensing, 104, 203–212.

[3] Bettinger, M., Martinis, S., & Plank, S.M., 2018. An automatic process chain for detecting burn scars using Sentinel-2 data. Southeastern European Journal of Earth Observation and Geomatics, submitted.

[4] PHAROS Project on a Multi-Hazard Open Platform for Satellite Based Downstream Services, http://cordis.europa.eu/project/rcn/188829_en.html [last accessed in April 2020].

[5] R&T CNES R-S15 / OT-0004-083, 2015-2018. "Extraction of information from multi-source flows, applied to water surfaces".

[6] Martinis, S., Clandillon, S., Plank, S., Twele, A., Huber, C., Caspard, M., Maxant, J., Cao, W., Haouet, S., Fuchs, E.-M., 2017. ASAPTERRA - Advancing SAR and Optical Methods for Rapid Mapping. Final report, pp. 227.

[7] Tomás, R. et al., 2019 : Semi-automatic identification and pre-screening of geological–geotechnical deformational processes using persistent scatterer interferometry datasets- Remote Sensing, 11 (14), 1675.

[8] IWG-SEM Emergency Mapping Guidelines - Fire Chapter, 2018 (based on UNISTRA developments in HEIMDALL and past projects).

[9] Martinis, S., Kuenzer, C., Twele, A., 2015: Flood studies using Synthetic Aperture Radar data. In Thenkabail, P. (Ed.): Remote Sensing Handbook Vol. III, Remote Sensing of Water Resources, Disasters and Urban Studies, Taylor & Francis, London, UK, 145-173.

[10] Schumann, G., Hostache, R. Puech, C. Hoffmann, L. Matgen, P. Pappenberger, F. & Pfister, L., 2007. High-resolution 3-D flood information from radar imagery for flood hazard management. IEEE Transactions on Geoscience and Remote Sensing, 45, 1715–1725.

[11] Martinis, S., Twele, A. & Voigt, S., 2009. Towards operational near real-time flood detection using a split-based automatic thresholding procedure on high resolution TerraSAR-X data. Natural Hazards and Earth System Sciences 9, 303–314.

[12] Pulvirenti, L., Chini, M., Marzano, F.S., Pierdicca, N., Mori, S., Guerriero, L., Boni, G., Candela, L., 2012. Detection of floods and heavy rain using Cosmo–SkyMed data: the event in Northwestern Italy of November 2011. IEEE International Geoscience and Remote Sensing Symposium (IGARSS 2012), Munich, 22–27 July, 3026–3029.

[13] Matgen, P., Hostache, R., Schumann, G., Pfister, L., Hoffman, L., Svanije, H.H.G., 2011. Towards and automated SAR based flood monitoring system: lessons learned from two case studies. Phys. Chem. Earth 36 (7–8), 241–252.

[14] Schumann, G., Di Baldassarre, G., Alsdorf, D., Bates, P.D., 2010. Near real-time flood wave approximation on large rivers from space: application toe the River Po, Italy. Water Resour. Res. 46 (5), 1–8.

[15] eoPortal Directory, https://directory.eoportal.org/web/eoportal/satellite-missions/t/terrasar-x [last accessed in June 2018].

[16] Torres, R., Snoeij, P., Geudtner, D., Bibby, D., Davidson, M., Attema, E., Potin, P. et al., 2012. GMES Sentinel-1 Mission. Remote Sensing of Environment, 120: 9–24.

[17] Kittler, J., Illingworth, J., 1986. Minimum error thresholding. Pattern Recognition, 19 (1), 41-47.

[18] SWBD, 2005. Shuttle radar topography mission water body data set. https://dds.cr.usgs.gov/srtm/version2_1/SWBD/ [last accessed in June 2018].

[19] Carroll, M., Townshend, J., DiMiceli, C., Noojipady, P., Sohlberg, R., 2009. A new global raster water mask at 250 meter resolution. International Journal of Digital Earth 2 (4), 291–308.

[20] Rennó, C. D., Nobre, A. D., Cuartas, L. A., Soares, J. V., Hodnett, M. G., Tomasella, J. & Waterloo, M. J., 2008. HAND, a New Terrain Descriptor Using SRTM-DEM: Mapping Terra-Firme Rainforest Environments in Amazonia. Remote Sensing of Environment, 112 (9): 3469–3481.

[21] Lehner, B., Verdin, K. & Jarvis, A., 2008. New global hydrography derived from spaceborne elevation data. Eos, Transactions American Geophysical Union 89 (10): 93–94.

[22] Xiong, D., 2001. Automated Road Network Extraction from High Resolution Images. National Consortia on Remote Sensing in Transportation, Technical Notes, 3.

[23] Nevatia, R., Babu, K. R., 1980. Linear feature extraction and description. Computer Graphics and Image Processing. Computer Graphics and Image Processing, 13, 257-269.

[24] Mingjun, S., Daniel, C., 2004. Road extraction using SVM and image segmentation. Photogrammetric Engineering & Remote Sensing, 70, 1365-1371.

[25] Boggess, J. E., 1993: Identification of roads in satellite imagery using artificial neural networks: A contextual approach. Technical Report: MSU-930815, Mississippi State University.

[26] Roberts, D., Gardner, M., Funk, C., Noronha, V., 2001: Road extraction using mixture and Q-tree filter techniques. National Center for Geographical Information & Analysis, University of California at Santa Barbara, http://www.ncgia.ucsb.edu/ncrst/research/reports/1Q3supplement-p.pdf.

[27] Karunanithi, N., Greeney, W. J., Whitley, D., Bovee, K., 1994: Neural networks for river flow prediction. Journal of Computing in Civil Engineering, 8(2), 201–220.

[28] Vapnik, V. N., 1995: The Nature of Statistical Learning Theory. Springer-Verlag.

[29] Vapnik, V. N., 1998: Statistical Learning Theory. Wiley.

[30] Cherkassky, V., Mulier, F. M., 1998: Learning from Data: Concepts, Theory, and Method. John Wiley & Sons.

[31] Cortes, C., Vapnik, V., 1995: Support-vector networks. Machine Learning 20, 273-297.

[32] Tobler, Waldo. 1987: “Measuring Spatial Resolution”, Proceedings, Land Resources Information Systems Conference, Beijing, pp. 12-16.

[33] Pekel, J.-F., Cottam, A., Gorelick, N., Belward, A. S.: High-resolution mapping *of* global surface water *and* its long-term changes. Nature 540, 418-422 (2016). (doi:10.1038/nature20584)

[34] Santurri, L. Carlà, R., Fiorucci, F., Aiazzi, B., Baronti, S., Cardinali, M., Mondini, A., 2010: Assessment of very high resolution satellite data techniques for landslide recognition. Int. Arch. Photogramm. Remote Sens. Spat. Inf. Sci, 38/B7, 492-496.

[35] Fiorucci, F., Cardinali, M., Carlà, R., Rossi, M., Mondini, A.C., Santurri, L., Ardizzone, F., Guzetti, F., 2011: Seasonal landslide mapping and estimation of landslide mobilization rates using aerial and satellite images. Geomorphology, 129, 59-70.

[36] Nichol, E.J., Shaker, A., Wong, M.-S., 2006: Application of high-resolution stereo satellite images to detailed landslide hazard assessment. Geomorphology, 76.

[37] Notti, D., Herrera, G., Bianchini, S., Meisina, C., García-Davalillo, J.C., Zucca, F., 2014: A methodology for improving landslide PSI data analysis. Int. J. Remote Sens. 2014, 35, 2186–2214.

[38] Key, C.H., Benson N., Ohlen D., Howard S., McKinley R., Zhu Z., 2002: The normalized burn ratio and relationships to burn severity: ecology, remote sensing and implementation. Proceedings of the Ninth Forest Service Remote Sensing Applications Conference. American Society for Photogrammetry and Remote Sensing, Bethesda, MD, J.D. Greer, ed. Rapid Delivery of Remote Sensing Products.

[39] Herrera, G., Davalillo, J.C., Mulas J., Cooksley G., Monserrat O., Pancioli V. 2009: Mapping and monitoring geomorpho-logical processes in mountainous areas using PSI data: Central Pyrenees case study. Nat. Hazard Earth Syst. Sci., 9: 1587-1598.

[40] Barra A., Monserrat, O., Mazzanti, P., Esposito, C., Crosetto, M., Mugnozza, G. 2016: First insights on the potential of Sentinel-1 for landslides detection, Geomatics, Natural Hazards and Risk, 7 (6), 1874-1883.

[41] Massonnet, D., Feigl, K.L. 1998: Radar interferometry and its application to changes in the Earth's surface. Rev. Geophys., 36, 441-500.

[42] Rosen, P.A. 2000: Synthetic aperture radar interferometry. Proceedings of IEEE, 88, (3), 333-382.

[43] Berardino, P., Fornaro, G., Lanari, R. 2002: A new algorithm for surface deformation monitoring based on small baseline differential SAR interferograms. IEEE Transactions on Geoscience and Remote Sensing, 40 (11), 2375-2382.

[44] Mora O., Mallorqui, J.J., Broquetas, 2003. A Linear and nonlinear terrain deformation maps from a reduced set of interferometric SAR images. IEEE Transactions on Geoscience and Remote Sensing, 41, 2243–2253.

[45] Ferretti, A., Monti-Guarnieri, A., Prati, C., Rocca, F., Massonet, D. 2007: InSAR principles-guidelines for SAR interferometry processing and interpretation, 19. The Netherlands: ESA Publications.

[46] Tomas R.T., Romero, R., Mulas, J., Marturià, J., Mallorquí, J., Lopez-Sanchez, J.M., Herrera, G., Gutiérrez, F., González, P.J., Fernández, J., Duque, S., Concha-Dimas, A., Cocksley, G., Castañeda, C., Carrasco, D., Blanco, P. 2014: Radar interferometry techniques for the study of ground subsidence phenomena: a review of practical issues through cases in Spain Environmental earth sciences, 71 (1), 163-181.

[47] Crosetto, M., Monserrat, O., Cuevas-González, M., Devanthéry, N., Crippa, B. 2016: Persistent scatterer interferometry: A review. ISPRS J. Photogramm. Remote Sens. 2016, 115, 78–89.

[48] Description of the procedure to generate the ADA and VEAM, Deliverable D2.4: Geohaz 783169U project http://www.icgc.cat/en/Innovation/R-D-i-projects/U-Geohaz [last accessed in August 2018].

[49] Malamud, B.D.,Turcotte, D.L., Guzzetti, F., Reichenbach, P. 2004: Landslide inventories and their statistical properties. Earth Surf. Process. Landf., 29 (6), 687-711, 10.1002/esp.1064.

[50] Martha, T.R., Kerle, N., Jetten, V., van Westen, C., Vinod Kumar, K., 2010: Characterising spectral, spatial and morphometric properties of landslides for semi-automatic detection using object-oriented methods, Geomorphology, 116, 24-36.

[51] Danneels, G., Pirard, E., & Havenith, H.-B., 2007: Automatic landslide detection from remote sensing images using supervised classification methods. International Geoscience and Remote Sensing Symposium 2007, 3014-3017.

[52] Lu, P., Stumpf, A., Kerle, N., Casagli, N. 2011: Object-oriented change detection for landslide rapid mapping. IEEE Geoscience and Remote Sensing Letters, 8 (4), 701-705.

[53] Stumpf, A., Lachiche, N., Malet, J.P., Kerle, N., Puissant, A., 2014: Active learning in the spatial domain for remote sensing classification, IEEE Trans. Geosci. Remote Sens., 52, 2492-2507.

[54] Golovko, D., Roessner, S., Behling, R., Wetzel, H.-U., Kaufmann, H.: GIS-based integration of heterogeneous data for a multi-temporal landslide inventory. In Landslide Science for a Safer Geoenvironment; Sassa, K., Canuti, P., Yin, Y., Eds.; Springer: Berlin, Germany, 2014; 799–804.